Runt-related transcription factor 1 is required for murine osteoblast differentiation and bone formation

Received for publication, February 5, 2019, and in revised form, April 16, 2020 Published, Papers in Press, June 22, 2020, DOI 10.1074/jbc.RA119.007896

Jun Tang[1,2,‡], Jing Xie[2,3,‡], Wei Chen[2,*], Chenyi Tang[2], Jinjin Wu[2], Yiping Wang[2], Xue-Dong Zhou[3], Hou-De Zhou[1,*], and Yi-Ping Li[2,*]

From the [1]Department of Metabolism & Endocrinology, Hunan Provincial Key Laboratory of Metabolic Bone Diseases, National Clinical Research Center for Metabolic Diseases, The Second Xiangya Hospital, Central South University, Changsha, Hunan, People's Republic of China, the [2]Department of Pathology, the University of Alabama at Birmingham School of Medicine, Birmingham, Alabama, USA, and [3]The State Key Laboratory of Oral Diseases, West China College of Stomatology, Sichuan University, Chengdu, Sichuan, People's Republic of China

Edited by Xiao-Fan Wang

Despite years of research investigating osteoblast differentiation, the mechanisms by which transcription factors regulate osteoblast maturation, bone formation, and bone homeostasis is still unclear. It has been reported that runt-related transcription factor 1 (*Runx1*) is expressed in osteoblast progenitors, pre-osteoblasts, and mature osteoblasts; yet, surprisingly, the exact function of RUNX1 in osteoblast maturation and bone formation remains unknown. Here, we generated and characterized a pre-osteoblast and differentiating chondrocyte-specific *Runx1* conditional knockout mouse model to study RUNX1's function in bone formation. *Runx1* ablation in osteoblast precursors and differentiating chondrocytes via osterix-Cre (Osx-Cre) resulted in an osteoporotic phenotype and decreased bone density in the long bones and skulls of *Runx1$^{f/f}$Osx-Cre* mice compared with *Runx1$^{f/f}$* and *Osx-Cre* mice. RUNX1 deficiency reduced the expression of SRY-box transcription factor 9 (SOX9), Indian hedgehog signaling molecule (IHH), Patched (PTC), and cyclin D1 in the growth plate, and also reduced the expression of osteocalcin (OCN), OSX, activating transcription factor 4 (ATF4), and RUNX2 in osteoblasts. ChIP assays and promoter activity mapping revealed that RUNX1 directly associates with the *Runx2* gene promoter and up-regulates *Runx2* expression. Furthermore, the ChIP data also showed that RUNX1 associates with the *Ocn* promoter. In conclusion, RUNX1 up-regulates the expression of *Runx2* and multiple bone-specific genes, and plays an indispensable role in bone formation and homeostasis in both trabecular and cortical bone. We propose that stimulating *Runx1* activity may be useful in therapeutic approaches for managing some bone diseases such as osteoporosis.

Bone marrow mesenchymal stem cells are multipotent progenitors that give rise to osteoblasts, chondrocytes, and adipocytes upon specific stimulation for cell differentiation. Notably, the majority of bone disease conditions associated with bone loss, such as osteoporosis, result from impaired osteoblast function and disrupted bone homeostasis. Despite years of research in osteoblast lineage and osteoblast differentiation, the mechanisms by which transcription factors regulate bone homeostasis is unclear, even though an imbalance of bone homeostasis is significant to a number of diseases (1–3). A complete understanding of the mechanisms by which transcription factors control bone formation to maintain bone homeostasis is critical to developing therapies for the often-debilitating disorders of skeletal insufficiency (*e.g.* osteoporosis, periodontal disease, and tumor metastasis to bone).

The RUNX (Runt-related transcription factor) family is composed of RUNX1, RUNX2, and RUNX3, which play important roles in cell lineages (4). RUNX1 regulates hematopoietic stem cell differentiation into mature blood cells (5), and plays a major role in developing pain-transmitting neurons (6). RUNX1 has been reported to be involved in cartilage formation and fracture healing (7–9). In addition, others have explored the role of RUNX1 in the commitment and differentiation of chondroprogenitor cells into the chondrogenic lineage (9, 10). Although Runx1 has been reported to be expressed in osteoblast progenitors, pre-osteoblasts, and mature osteoblasts, the function of RUNX1 in osteoblasts has not yet been investigated (11). RUNX2 determines commitment to the osteoblastic lineage (12–15), and interacts with many co-regulators and transcription factors in the transcriptional regulation of its target genes (16). However, previous reports have shown that overexpression of *Runx2* in cells of the osteoblastic lineage leads to an osteopenia phenotype due to negative regulation of osteoblast maturation (17). Thus, there is an urgent need to characterize transcription factor(s) that positively regulate osteoblast maturation and bone formation for healthy bone homeostasis to develop novel and efficient therapeutic approaches to treat bone diseases, including osteoporosis. RUNX1, a regulator of both *Runx2* and bone genes, could facilitate the design of safer and novel therapeutic approaches for osteoporosis. *Runx1* expression precedes *Runx2*, indicating its importance in cell lineage determination (11). Notably, it was previously reported that the overlapping expression of *Runx1* and *Runx2* supports cooperative induction of skeletal development (18). Furthermore, the *Runx1* expression profile indicates that RUNX1 may have positive regulatory functions in osteoblasts that support bone formation for bone hemostasis. However, the function of RUNX1 in bone formation to maintain bone homeostasis, and how RUNX2 is regulated by RUNX1 is still largely unclear.

This article contains supporting information.

‡These authors contributed equally to this work.
*For correspondence: Wei Chen, weichen@uabmc.edu; Hou-De Zhou, houdezhou@csu.edu.cn; Yi-Ping Li, yipingli@uabmc.edu.

To investigate the role of RUNX1 in postnatal-skeletal development, we utilized *Osterix*-Cre *(Osx*-Cre*)* to specifically delete *Runx1* in osteoblast precursors and differentiating chondrocytes (19, 20). We found that *Runx1* deletion in osteoblast precursors and differentiating chondrocytes leads to a severe osteoporotic phenotype with a 50% reduction in both total bone volume and cortical bone, and a 40% reduction in trabecular bone. In this study, we have revealed that RUNX1 plays an indispensable role in postnatal skeletal development and bone homeostasis via directly associating with the *Runx2* and *Ocn* promoters and regulating *Runx2* and *Ocn* expression directly. Our results have revealed the important functions of RUNX1 in bone formation and the mechanisms underlying how RUNX1 maintains bone homeostasis, indicating that targeting RUNX1 may result in novel therapeutic approaches for degenerative bone diseases such as osteoporosis.

Results

Runx1$^{f/f}$Osx-Cre mice exhibit shortened limbs, hypoplastic skeletons, and osteoporotic phenotype due to impaired bone mineralization

To investigate the role of RUNX1 in osteoblast development during postnatal skeletogenesis, we generated *Runx1$^{f/f}$Osx*-Cre mice, deleting the *Runx1* gene specifically in the osteoblast lineage. *Runx1$^{f/f}$Osx-Cre* mice survived into adulthood, but the homozygote mice displayed severe skeletal defects characterized by shorter stature (Fig. 1*A*). PCR was used to confirm the genotypes of the mice (Fig. 1*B*). Through immunohistochemical (IHC) staining, we detected *Runx1* expression in the trabecular bone of 14-week–old mice, which showed *Runx1* was efficiently deleted in osteoblasts (Fig. 1*C*). X-ray analysis was performed to assess the bone density of *Runx1$^{f/f}$Osx-Cre* and control mice (Fig. 1*D*). Radiographic analysis of 13-week–old *Runx1$^{f/f}$Osx-Cre* and control skulls (Fig. 1*D,* Fig. S1*C*) and femurs (Fig. 1*D,* Fig. S1*A*) revealed a significant decrease in ossification and bone density, as well as mandibular defects in *Runx1$^{f/f}$Osx-Cre* mice (Fig. 1*D*). Notably, *Runx1$^{f/f}$Osx-Cre* mice had a significantly lower bone density in both the long bones and the calvarial area (Fig. 1*D,* Fig. S1*A*, *white arrows*). Micro-computed tomography (μCT) analysis of 14-week–old male and female *Runx1$^{f/f}$Osx-Cre* femurs revealed a significant decrease in bone volume/tissue volume, trabecular number, trabecular thickness, and cortical bone compared with control (Fig. 1*E*). Both the cortical bone and total bone volume were reduced by 50% in the *Runx1$^{f/f}$Osx-Cre* mice, whereas the trabecular bone was reduced by 40% (Fig. 1, *E* and *F*). These results demonstrated that Runx1 ablation in osteoblasts and chondrocyte precursors results in an osteoporotic phenotype characterized by short stature and impaired bone mineralization. Alizarin red and Alcian blue staining revealed that, except for the vertebrae and sternum, the bones in the newborn *Runx1$^{f/f}$Osx-Cre* mice were severely underdeveloped (Fig. S2). Previous studies have indicated that Osx-cre mice have delayed calvarial ossification but no difference in the limbs (21, 22), which is consistent with our results (Fig. S2, *H–K*). Notably, we found that the newborn *Runx1$^{f/f}$Osx-Cre* mice exhibited severe skull bone loss in the cranium and cranial base compared with controls (Fig. S2, *A* and *B*). Moreover, compared with *Runx1$^{f/f}$* and *Osx-Cre* controls, *Runx1$^{f/f}$Osx-Cre* mice exhibited shorter and underdeveloped forelimbs (Fig. S2*C*), clavicles (Fig. S2*D*), and hind limbs (Fig. S2*E*). Overall, the skeletons of the *Runx1$^{f/f}$Osx-Cre* mice were severely underdeveloped and displayed an osteoporotic phenotype.

Runx1$^{f/f}$Osx-Cre newborn femurs have impaired endochondral and intramembranous bone ossification and decreased osteoblast numbers

In further analyzing the growth retardation observed in the *Runx1$^{f/f}$Osx-Cre* mice, we performed hematoxylin and eosin (H&E), Von Kossa, alkaline phosphatase (ALP), and tartrate-resistant acid phosphatase (TRAP) staining on femurs from newborn mice. H&E stain showed that newborn *Runx1$^{f/f}$Osx-Cre* mice had decreased ossification and endochondral bone formation, as well as reduced cell density and a 50% decrease in osteoprogenitor cells in the periosteum (Fig. 2, *A* and *F*, *red arrows*). These osteoprogenitor cells differentiate into the first osteoblasts and produce a bone collar, which becomes the future cortical bone. Thus the 2-fold decrease in cortical bone width seen in *Runx1$^{f/f}$Osx-Cre* may be due to the 50% decrease of the cells in the periosteum. ALP stain showed that osteoblast formation was significantly reduced in the *Runx1$^{f/f}$Osx-Cre* mice compared with *Osx-cre* and WT mice, whereas there were significantly fewer ALP-positive cells within the periosteum (Fig. 2, *B* and *E*); we found a 3-fold decrease in ALP-positive cells in *Runx1$^{f/f}$Osx-Cre* mice, which led to the reduction in both trabecular and cortical bone. Notably, the width of the cortical bone was reduced by 50% in *Runx1$^{f/f}$Osx-Cre* mice (Fig. 2*B*). Von Kossa staining revealed a 50% decrease in osteoblast mineralization as well as a significantly shorter medullary cavity in newborn *Runx1$^{f/f}$Osx-Cre* mice compared with *Osx-cre* and WT mice (Fig. 2, *C*, *E*, and *F*). Finally, TRAP staining confirmed that there were no significant differences in osteoclast numbers between WT and *Runx1$^{f/f}$Osx-Cre* mice in both newborn and at the 3-week–old mice (Fig. 2, *D* and *E,* Fig. S3, *A* and *B*), demonstrating that the reduced bone density in *Runx1$^{f/f}$Osx-Cre* mice was not due to an increase in osteoclast proliferation. Collectively, these results demonstrate that bone formation is impaired in *Runx1$^{f/f}$Osx-Cre* mice, whereas osteoclast formation is not affected.

RUNX1 deficiency affects the cortical and trabecular bone formation in the Runx1$^{f/f}$Osx-Cre mice

Notably, we found that *Runx2* expression in newborn *Runx1$^{f/f}$Osx-Cre* mouse femurs decreased by 90% in the bone collar, and by 80% in the trabecular bone, whereas *Runx2* expression in the hypertrophic zone was not significantly changed (Fig. 3, *A* and *B*). Notably, the width of the cortical bone was decreased by 50% in the newborn *Runx1$^{f/f}$Osx-Cre* mouse femurs (Fig. 3*B*). To further study the effects of RUNX1 deficiency on bone homeostasis, we compared the mineral apposition rate in *Runx1$^{f/f}$Osx-Cre* mice with their sex-matched littermate controls via double calcein labeling (Fig. S3*E*). The results demonstrated that the mineral apposition rate was decreased by 2-fold in the *Runx1$^{f/f}$Osx-Cre* mice

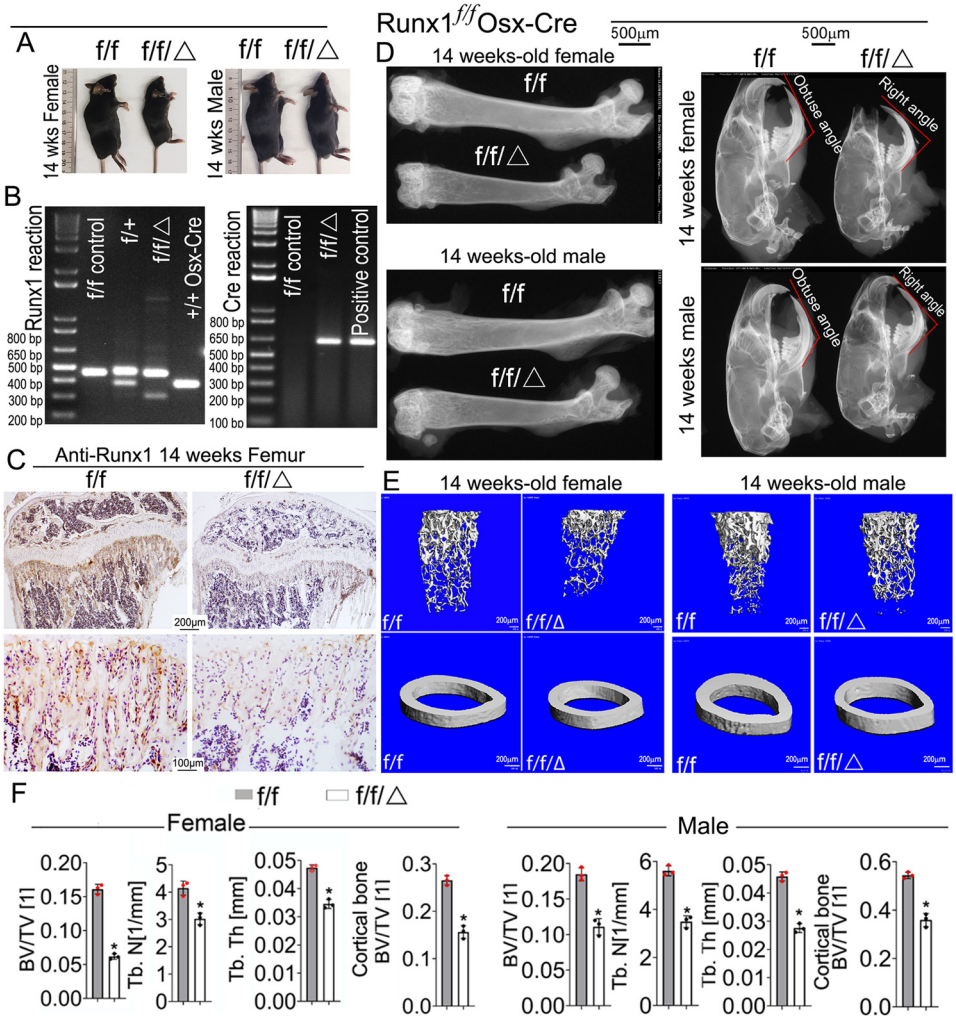

Figure 1. *Runx1$^{f/f}$Osx-Cre* mice have decreased bone mineralization and skeletal deformities. *A,* photographic images of 14-week–old ($n = 16$) *Runx1$^{f/f}$Osx-Cre* (*f/f/Δ*) mice and WT (*f/f*) mice. *B,* PCR was used to determine *Runx1* alleles (*f/f*, *f/+*, *+/+*, or deletion) and the presence of Cre. *C,* IHC staining of 14-week–old Runx1$^{f/f}$*Osx-Cre* (*f/f/Δ*), and WT (*f/f*) mice tibias using RUNX1 antibody. *D,* x-ray analysis of 14-week-old male and female femurs and skulls, $n = 19$. *E,* μCT scans of femurs from 14-week-old male and female mice, $n = 3$. *F,* quantification of *E*. Results are expressed as mean ± S.D.; *, $p < 0.05$.

compared with the control, leading to the low bone density seen in the mutant mice. Furthermore, we found that the P1NP serum level (bone formation marker) was reduced by 2-fold in the *Runx1$^{f/f}$Osx-Cre* mice, indicating that bone formation rate was affected by *Runx1* CKO (Fig. 3*C*). Thus, RUNX1 plays an important role in up-regulating *Runx2* expression in precursor cells and bone formation, and RUNX1 deficiency leads to significantly reduced cortical and trabecular bone.

RUNX1 deficiency affects the chondrocyte proliferation and maturation in the long bone of Runx1$^{f/f}$Osx-Cre mice

Endochondral bone formation originates from cartilage templates, which are then replaced by bone (23). The delayed endochondral ossification observed in the *Runx1f/fOsx-Cre* mice prompted us to examine the impact of the *Osx*-Cre–mediated *Runx1* deletion on the development of the growth plate. Safranin O staining of femurs revealed a significant decrease in relative length of the growth plate, proliferating zone, and hypertrophic zone over the total length of the bone in the mutant mice (Fig. 4, *A* and *B*). Furthermore, the proliferative zone in *Runx1$^{f/f}$Osx-Cre* mice was shorter (Fig. 4*A*). We compared expression levels of *Col2a1* and *Col10a1* in the growth plate, which are specific collagens produced by proliferative and hypertrophic chondrocytes. We found that expression levels of both *Col2a1* and *Col10a1* were significantly decreased in the growth plate in *Runx1$^{f/f}$Osx-Cre* mice (Fig. 4, *C*, *D*, and *F*). Upon staining to detect proliferating cell nuclear antigen (PCNA), we found that the expression was significantly decreased in both the proliferative and hypertrophic zones of *Runx1$^{f/f}$Osx-Cre* mice (Fig. 4, *E* and *F*). These results indicate that the decreased length of the long bones in *Runx1$^{f/f}$Osx-Cre* mice is due to reduced chondrocyte proliferation, which results in impaired growth plate development and trabecular bone formation.

Loss of Runx1 reduced the expression of Sox9, Ihh, cyclin D1, and Ptc in chondrocytes of Runx1$^{f/f}$Osx-Cre mice, and impaired Ihh-Cyclin D1 signaling

Cyclin D1 is among the Cyclin/CDK protein complexes that regulate the cell cycle, and as a target of Indian hedgehog (*Ihh*) plays an important role in chondrocyte proliferation (24). To

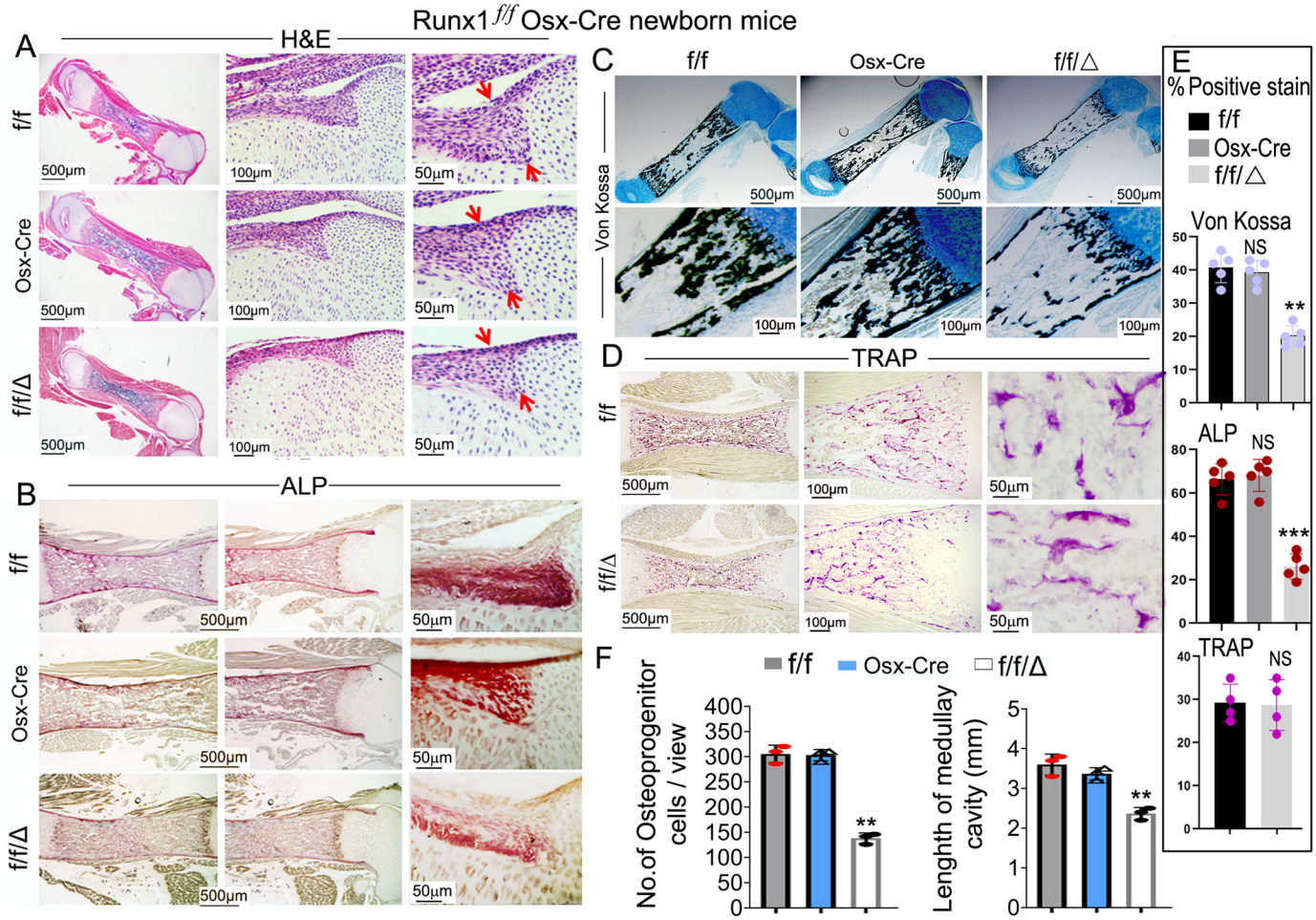

Figure 2. Endochondral bone ossification was significantly impaired and osteoblast numbers were largely decreased in *Runx1*$^{f/f}$*Osx-Cre* newborn mice femurs, but not in *Osx-Cre* newborn mice femurs compared with WT mice femurs. *A–D*, newborn *Runx1*$^{f/f}$*Osx-Cre* (f/f/Δ), *Osx-Cre* and WT (f/f) mice femurs were stained with (*A*) H&E stain, (*B*) ALP stain, (*C*) Von Kossa and Alcian blue stain, and newborn *Runx1*$^{f/f}$*Osx-Cre* (f/f/Δ) and WT (f/f) mice femurs were stained with (*D*) TRAP stain. *E*, histomorphometry of WT (f/f), *Osx-Cre* and *Runx1*$^{f/f}$*Osx-Cre* (f/f/Δ) mice ($n = 4$) showing ALP stain surface per bone surface (*BS*) area, Von Kossa stain surface per bone surface area, and TRAP stain surface per bone surface area. *F*, quantification of cells in the periosteum in *A* and length of the medullary cavity. Results are expressed as mean ± S.D. *NS*, not significant; **, $p < 0.01$; ***, $p < 0.001$.

address the mechanism underlying the effects of RUNX1 on chondrocytes, we examined the expression levels of SRY-related high mobility group-Box gene 9 (*Sox9*), *Cyclin D1*, *Ihh*, and Patched (*Ptc*) by immunofluorescent (IF) staining of femur sections from newborn mice (Fig. 5, *A–D*). Compared with WT mice, the expression of a key transcription factor in the chondrocyte lineage, *Sox9*, was decreased in *Runx1*$^{f/f}$*Osx-Cre* mice (Fig. 5, *A* and *F*). The expression of *Ihh*, which is important for the chondrocyte maturation, was reduced in *Runx1*$^{f/f}$*Osx-Cre* mice (Fig. 5, *B* and *F*). The expression of the IHH target gene, *Ptc*, was also reduced in the growth plates in *Runx1*$^{f/f}$*Osx-Cre* mice; *Ptc* expression was detected in the pre-hypertrophic zone in the growth plates of WT mice, but was greatly reduced in mutant mice (Fig. 5, *C* and *F*). Cyclin D1, a cell-cycle–regulating protein downstream of *Ihh* (24), was reduced in the proliferation zone of *Runx1*$^{f/f}$*Osx-Cre* mice femurs (Fig. 5, *D* and *F*), which may induce the inhibition of chondrocyte proliferation. Thus, *Runx1* plays an important role in pre-hypertrophic chondrocyte proliferation and differentiation. IF staining of newborn mice femurs showed that expression levels of both *Osx* and *Ocn*, genes critical to the skeletal formation, were decreased in *Runx1*$^{f/f}$*Osx-Cre* mice (Fig. 5, *E* and *F*). In conclusion, we found that RUNX1 deficiency affects chondrocyte proliferation by inhibiting Ihh-cyclin D1 signaling. Furthermore, we found that RUNX1 deficiency reduces the expression of genes critical in skeletal formation.

RUNX1 deficiency in primary calvarial cells inhibits osteoblastogenesis

We investigated the impact of *Runx1* deletion on osteoblastogenesis *in vitro* using calvarial cells from control and *Runx1*$^{f/f}$*Osx-Cre* mice, which were maintained in the osteogenic medium for 14 and 21 days. Calvarial cells from *Runx1*$^{f/f}$*Osx-Cre* mice after 14 days of culture showed reduced osteoblast formation, which was detected through ALP stain (Fig. 6*A*, Fig. S4*A*). The oil red O stain showed that adipocytes were increased in the *Runx1*$^{f/f}$*Osx-Cre* mice after 14 days of culture (Fig. S4, *B* and *C*). The reduction in mineralization observed in *Runx1*$^{f/f}$*Osx-Cre* mice was detected by Von Kossa staining after 21 days of culture (Fig. 6*A*, Fig. S4*A*). Through qPCR and Western blotting we analyzed the expression of several key factors that affect osteoblast

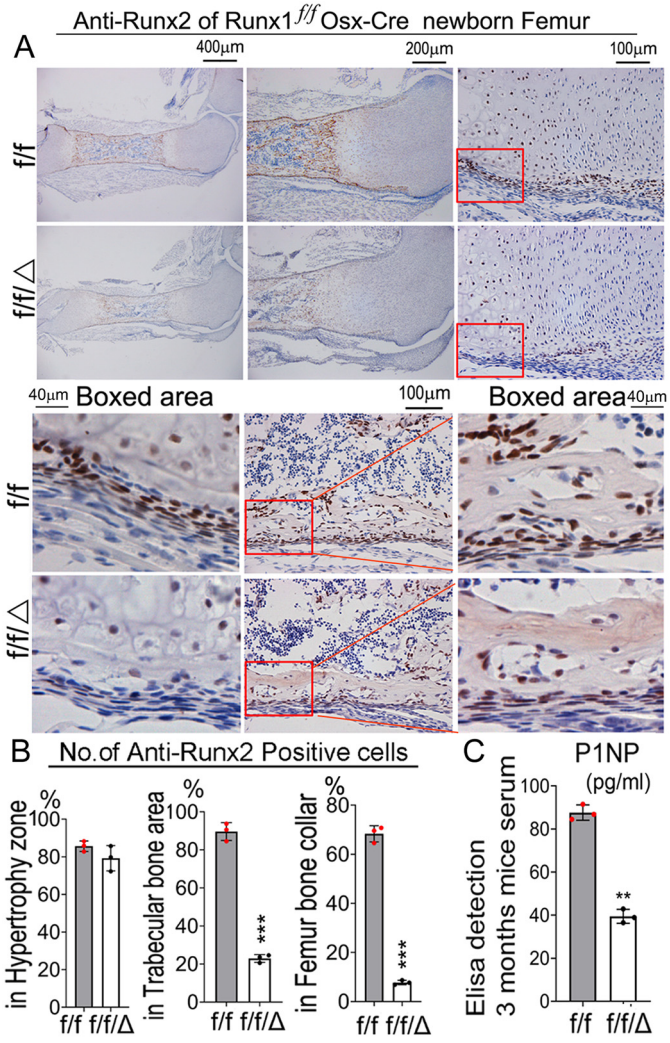

Figure 3. *Runx2* expression in bone is significantly decreased in *Runx1*$^{f/f}$*Osx-Cre* mice. *A*, IHC staining RUNX2 antibody of femur paraffin sections from P0 *Runx1*$^{f/f}$*Osx-Cre* (f/f/Δ) and WT (f/f) mice. *B*, quantification of *A*. *C*, ELISA detection of P1NP (pg/ml) in 3-month–old mouse serum indicating bone formation is affected by gene CKO. Results are expressed as mean ± S.D., $n = 3$ in each group. *, $p < 0.05$; **, $p < 0.01$; ***, $p < 0.001$.

differentiation and function in WT and *Runx1*$^{f/f}$*Osx-Cre* mice. Western blotting at days 7 and 14 of culture showed that protein levels of key bone genes *Runx1*, *Runx2*, *Osx*, and *Atf4* were all significantly reduced, whereas protein levels of CBFβ were unaffected (Fig. 6, *B* and *C*, Fig. S4*D*). AAV-mediated overexpression of Runx2 in *Runx1*$^{f/f}$*Osx-Cre* cells partially rescued osteoblast differentiation (Fig. S5*A*). The protein levels of RUNX1, RUNX2, OSX, ATF4, and OCN were detected by Western blotting (Fig. S5, *B* and *C*). Consistently, qPCR showed that RUNX1 deficiency significantly reduced the expression *Runx1*, *Runx2*, *Osx*, *Atf4*, and *Ocn* (Fig. 6*D*). We performed genome-wide expression analysis from day 14 cultured osteoblasts in osteoblast differentiation medium to examine the transcriptional profile related with *Runx1* knockdown. Our RNA-Seq analysis revealed significantly decreased expression levels of bone formation and homeostasis markers such as *Runx2*, *Osx*, *Dmp1*, *Alp*, and *Ocn* (Fig. 6*E*). We also found similar decreased signaling changes indicated by reduced *Pth1r* and *Ihh* expression (Fig. 6*E*). Our RNA-Seq data also revealed increased markers of adipogenesis in *Runx1* knockdown osteoblasts through up-regulated expression of *Pparg*, *Cebp*/α, and *Fabp4* (Fig. 6*E*). Taken together, these results demonstrate that *Runx1* deletion impacts osteoblast differentiation by affecting the expression of genes critical to osteoblast differentiation at the mRNA and protein levels. These data also indicate that osteoblasts generated from *Runx1*$^{f/f}$*Osx-Cre* mice were prevented from differentiating into mature osteoblasts.

RUNX1 up-regulates Runx2 and Ocn expression by directly associating with their promoters

ChIP assay was performed to elucidate if RUNX1 binds to the *Ocn* and *Runx2* promoters. We analyzed the respective promoter regions and designed primers accordingly. The RUNX1-binding sites in the *Ocn* promoter region (−4000/+200) were predicted (Fig. 7*A*). ChIP analysis was performed using the anti-RUNX1 antibody, and DNA was pulled down, amplified, and analyzed using primers. The ChIP input value using each primer represents the binding efficiency of an adjacent region around the location of the primer pair. We found that *Ocn* primer 2 resulted in the highest value, indicating that RUNX1-binding site 2 in the *Ocn* promoter region should be the most efficient (Fig. 7, *B* and *C*), and that RUNX1 potentially binds to the *Ocn* promoter around binding site 2 (Fig. 7*A*). We then examined the *Runx2* promoter and found several potential RUNX1-binding sites in the *Runx2* promoter region (−4000/+200) (Fig. 7*D*). We performed ChIP analysis using the anti-RUNX1 antibody, and DNA was pulled down, amplified, and analyzed using primers. We found that *Runx2* primer 2 resulted in the highest value, indicating that RUNX1-binding site 4 in the *Runx2* promoter region should be the most efficient (Fig. 7, *E* and *F*). This indicated that RUNX1 potentially binds to the *Runx2* promoter around binding site 4 (Fig. 7*D*). The promoter luciferase assay showed that luciferase activity was highest when driven by the longest *Runx2* promoter fragment (−2937/+80) and significantly lower (90% reduction) when driven by the other *Runx2* promoter fragments (Fig. 7*G*). In conclusion, our data demonstrated that RUNX1 associates with the *Ocn* and *Runx2* promoter regions and regulates their expression directly.

Discussion

In this study, we found that ablation of *Runx1* reduced the expression of *Sox9*, *Ihh*, *Ptc*, and *CyclinD1* in the growth plate, and impaired the proliferative and hypertrophic zones in the growth plate, whereas the trabecular bone was reduced by 40%, suggesting a central role of Runx1 in chondrocyte proliferation. *Runx1* ablation also reduced the expression of *Ocn*, *Osx*, *Atf4*, and *Runx2* in osteoblasts, and resulted in an osteoporotic phenotype in *Runx1*$^{f/f}$*Osx-Cre* mice. Deficiency of RUNX1 results in a 2-fold decrease in osteoprogenitor cells in the periosteum, subsequently leading to the lack of bone collar in the newborn *Runx1*$^{f/f}$*Osx-Cre* mice and 2-fold decrease in cortical bone width seen in 14-week–old *Runx1*$^{f/f}$*Osx-Cre* mice. Interestingly, our data demonstrate that the expression levels of *Runx2* and *Osx* are both decreased in the *Runx1*$^{f/f}$*Osx-Cre* mice. The expression of osteocalcin, a mature osteoblast

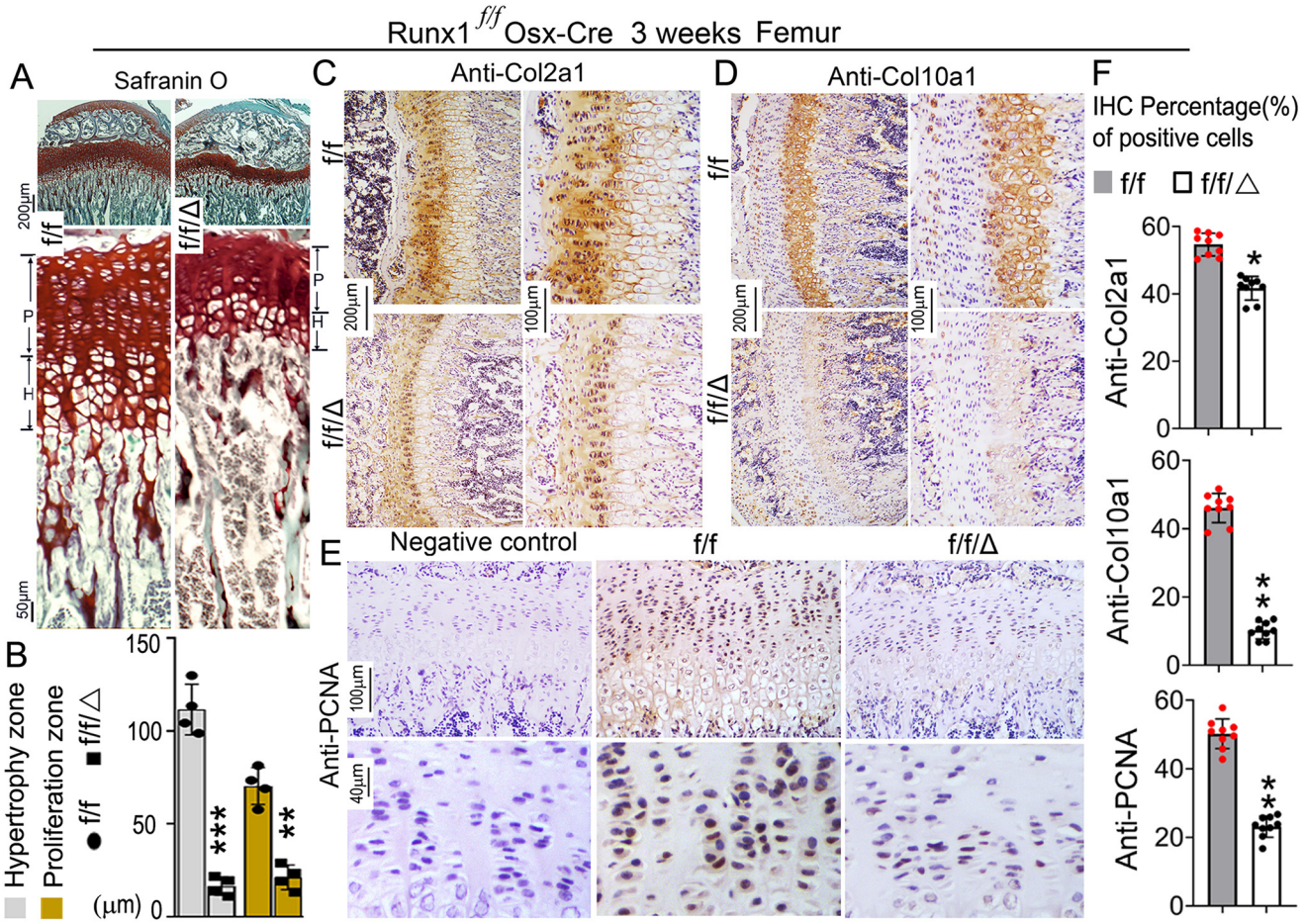

Figure 4. RUNX1 deficiency affects chondrocyte proliferation and maturation in *Runx1$^{f/f}$Osx-Cre* mice. *A,* safranin O staining of tibia and comparison of growth plate development between 3-week–old *Runx1$^{f/f}$Osx-Cre* and WT mice. *B,* quantification of hypertrophy zone and proliferation zone in *A. C–E,* IHC staining of tibia paraffin sections from 3-week–old *Runx1$^{f/f}$Osx-Cre* (*f/f/*Δ) and WT (*f/f*) mice using (*C*) Col2a1 antibody, (*D*) Col10a1 antibody, and (*E*) PCNA antibody. *F,* quantification of immunostaining positive cells of anti-Col2a1, anti-Col10a1, and anti-PCNA in *B-D*. Results are expressed as mean ± S.D., $n = 9$ in each group. *, $p < 0.05$; **, $p < 0.01$.

marker, was also decreased in the *Runx1$^{f/f}$Osx-Cre* mice. Our data demonstrate that *Runx1* plays a central role in promoting the commitment of osteoblast precursors into the osteoblast lineage. Our ChIP and luciferase assay show that RUNX1 can bind to the *Runx2* promoter, and our ChIP assay showed that RUNX1 can bind to the *Ocn* promoter, indicating that RUNX1 can up-regulate *Runx2* and *Ocn* expression directly.

Endochondral ossification and intramembranous ossification are two major modes of bone formation. Endochondral ossification is involved in the formation of long bones through a cartilage intermediate, whereas the intramembranous ossification directly forms the flat bone on the mesenchyme (25). Our results showed that the skull bone density was lower, the ALP and Von Kossa stain were decreased in the mutant mouse more than in the Osx-cre and *Runx1$^{f/f}$* control mice, which indicated that the intramembranous ossification was affected because of the impaired osteoblast activity. As for the lone bone ossification, both chondrocyte and osteoblast were affected in the mutant mouse, so the deletion of *Runx1* in both the chondrocyte and pre-osteoblast contributed to the endochondral ossification. Taken together, these results indicate that RUNX1 promotes osteoblast formation and differentiation to promote bone formation through up-regulating *Runx2* and bone genes.

Previous reports have demonstrated that *Runx1* is important for mesenchymal stem cell commitment to the early stages of chondrogenesis, and is required for chondrocyte lineage commitment and differentiation (9, 10, 26), whereas there may be a cross-regulation between *Runx1* and *Runx2* in chondrocytes (10). *Runx1* was found expressed *in vivo* in osteoblasts at the site of bone formation and chondroblasts at sites of cartilage growth (11), and it was previously reported that RUNX1 dose-dependently regulates endochondral ossification during skeletal development and fracture healing (9). Yet the role of RUNX1 in bone formation and bone homeostasis has not been previously reported. RUNX2 regulates the expression of *Ihh* and *Col10a1* in their respective layers in the growth plate (16). Our results show that the expression of *Runx2* was not significantly changed in the hypertrophic zone in newborn mice, however, 3-week–old mice displayed an impaired hypertrophic zone, as well as significantly reduced expression of *Col10a1*. Through ChIP assays and promoter activity mapping, we demonstrated that *Runx2* is directly up-regulated by RUNX1 at the transcriptional level. Furthermore, our ChIP data also showed that RUNX1 directly associates with the promoter of *Ocn*. Thus, RUNX1 regulates *Runx2* expression directly to regulate chondrocyte and osteoblast differentiation and terminal maturation.

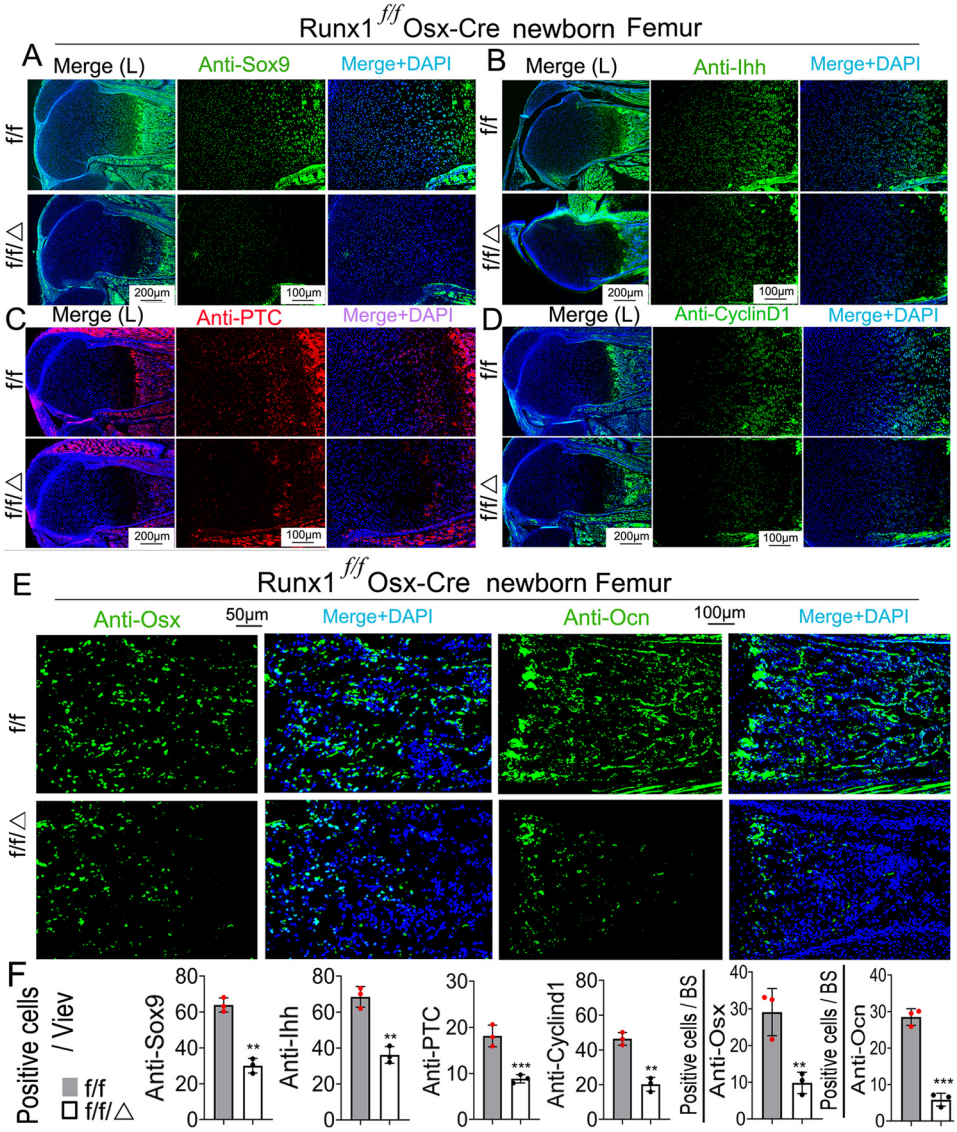

Figure 5. The expression of *Sox9*, *Ihh*, *Cyclin D1*, and *Ptc* in the growth plate, and the expression of *Ocn* in femurs were significantly decreased in *Runx1*$^{f/f}$*Osx-Cre* mice compared with WT mice. *A–D,* IF staining of the growth plates of P0 *Runx1*$^{f/f}$*Osx-Cre* mice compared with that of WT mice to detect (*A*) *Sox9*, (*B*) *Ihh*, (*C*) *Ptc*, and (*D*) *Cyclin D1*. *E,* IF staining with anti-Osterix, and anti-Ocn antibodies of femur frozen sections from P0 *Runx1*$^{f/f}$*Osx-Cre* (*f/f/*Δ) and WT (*f/f*) mice. *F,* quantification of *A–E*. Results are expressed as mean ± S.D., $n = 3$ in each group.

Lower bone mineral density and a 50% reduction in cortical thickness and 40% reduction in trabecular bone volume in the tibiae of *Runx1*$^{f/f}$*Osx-Cre* mice, which may be due to decreased osteoblast numbers in the bone collar, suggest that RUNX1 is required as an endogenous regulator of skeletal size and bone architecture. Kimura *et al.* (7) previously reported that in *Prx1 Runx1*$^{f/f}$ mice, aside from delay in sternal development, no other skeletal elements of the mice showed any abnormalities, however, their analysis was limited to P0 to 3-week–old mice using *Prx1* Cre. In our study, we examined mice from P0 to 14 weeks old to determine the role of *Runx1* in maintaining bone homeostasis. Our data demonstrate that *Runx1*$^{f/f}$*Osx-Cre* mice exhibited slower bone mineralization and bone formation rates, leading to lower bone density. These results suggest that RUNX1 is important for intramembranous and endochondral ossification. Interestingly, we found that *Runx1*$^{f/f}$*Osx-Cre* mice also displayed a mandibular defect characterized by a smaller angle of the lower jaw. The growth plate is the specialized cartilaginous structure for the longitudinal growth of bones (27). Fibril-forming type II collagen is the major collagen type in the growth plate, whereas hypertrophic chondrocytes in the growth plate produce type X collagen (27). We found that COL2a1 and COL10a1, which are produced by the proliferative and hypertrophic chondrocytes, were decreased in the mutant mice. Runx1 is involved in chondrocyte proliferation and lineage determination (28), and whereas *Runx1* is only expressed in the proliferative and resting chondrocytes, *Runx2* is expressed primarily by hypertrophic chondrocytes of the growth plates (29). Thus, following conditional deletion of *Runx1*, proliferative and resting chondrocytes cannot differentiate into hypertrophic chondrocytes due to the loss of *Runx2* regulation, leading to the significant reduction in trabecular bone observed in *Runx1*$^{f/f}$*Osx-Cre* mice. Moreover, the expression of PCNA was decreased in *Runx1*$^{f/f}$*Osx-Cre* mice. Thus, the

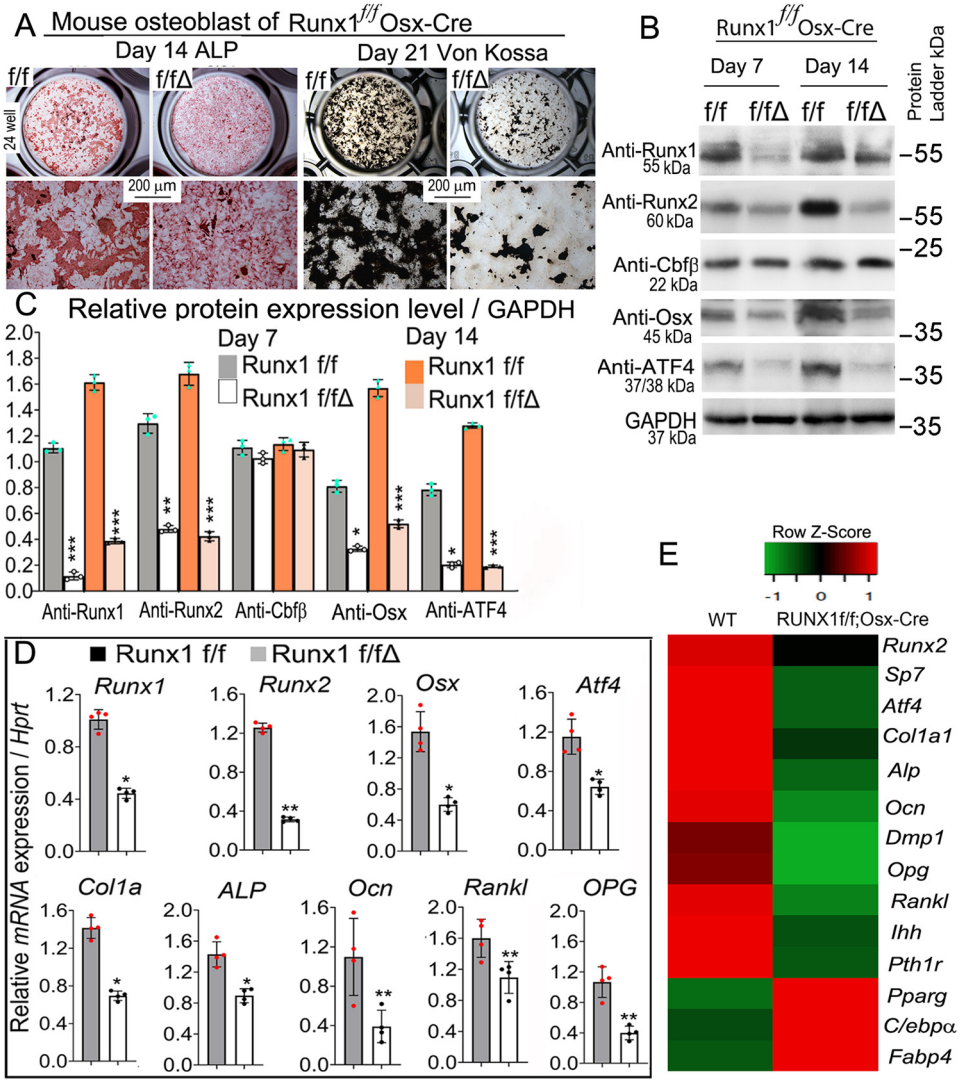

Figure 6. RUNX1 deficiency in primary calvarial cells cultured from *Runx1$^{f/f}$Osx-Cre* mice inhibits osteoblastogenesis. *A,* calvarial cells from *Runx1$^{f/f}$Osx-Cre* (f/f/Δ) and WT (f/f) newborn mice were cultured in osteogenic medium for 14 and 21 days, followed by ALP and Von Kossa stain, respectively. *B,* protein levels of Runx1, Runx2, Cbfβ, Osx, and Atf4 were analyzed by Western blotting analysis on days 7 and 14. GAPDH is shown as a control. *C,* quantification of *B. D,* qPCR analysis of mRNA expression levels of Runx1, Runx2, Osx, Atf4, ALP, *Col1α1, Ocn, Opg,* and *RANKL* in calvaria-derived osteoblasts from *Runx1$^{f/f}$Osx-Cre* (f/f/Δ) and WT (f/f) mice. *E,* RNA-Seq analysis of the osteoblasts cultured for 14 days in osteoblast differentiation medium showed decreased osteoblast gene expression and increased adipocyte formation genes expression. Heat map analysis of differentially expressed genes with at least a 2-fold change and controlled by adjusted *p* value of 0.05, as comparing osteoblasts of WT and *Runx1$^{f/f}$Osx-Cre*. In the heat map, *red* indicates up-regulation, whereas *green* indicates down-regulation. Select genes are listed separately. Results are expressed as mean ± S.D., $n \geqq 3$ in each group. *N.S.*, not significant; *, $p < 0.05$; **, $p < 0.01$; ***, $p < 0.001$.

shorter stature of the mice may be due to the inhibition of the chondrocyte differentiation and terminal maturation. Given the reduced numbers of proliferative and hypertrophic chondrocytes, osteoblasts, and reduced trabecular bone in *Runx1$^{f/f}$Osx-Cre* mice, *Runx1* may maintain trabecular bone formation through its regulation of *Runx2*, *Sox9*, *Ihh*, *Ptc*, and *Cyclin D1* in hypertrophic chondrocytes.

Our data show that the expression levels of *Sox9*, *Ihh*, *Ptc*, and *Cyclin D1*, genes that are involved in chondrocyte differentiation, were decreased in *Runx1$^{f/f}$Osx-Cre* mice, suggesting a potential role of Runx1 in pre-hypertrophic chondrocyte proliferation and differentiation. SOX9 is a transcription factor of the SRY-related high mobility group box family of proteins, which is the nuclear factor that is required for chondrogenesis (30, 31). Although *Sox9* is dispensable for the initial formation of mesenchymal condensations, it necessary for the subsequent steps toward chondrocyte differentiation (32). A previous study showed that RUNX1 can directly regulate the expression of *Sox9* (9). IHH produced by pre- and early hypertrophic chondrocytes leads to chondrocyte proliferation (33). *Cyclin D1* plays an important role in chondrocyte proliferation and is a target of IHH (24). IHH, a major regulator of bone development, coordinating chondrocyte proliferation, chondrocyte differentiation, and osteoblast differentiation, also binds to membrane protein PTC (34–37). Thus, *Runx1* regulates the early stages of the chondrocyte differentiation, whereas *Runx2* is important for the chondrocyte maturation (16). Furthermore, *Ihh* signaling in mature osteoblasts controls bone resorption by

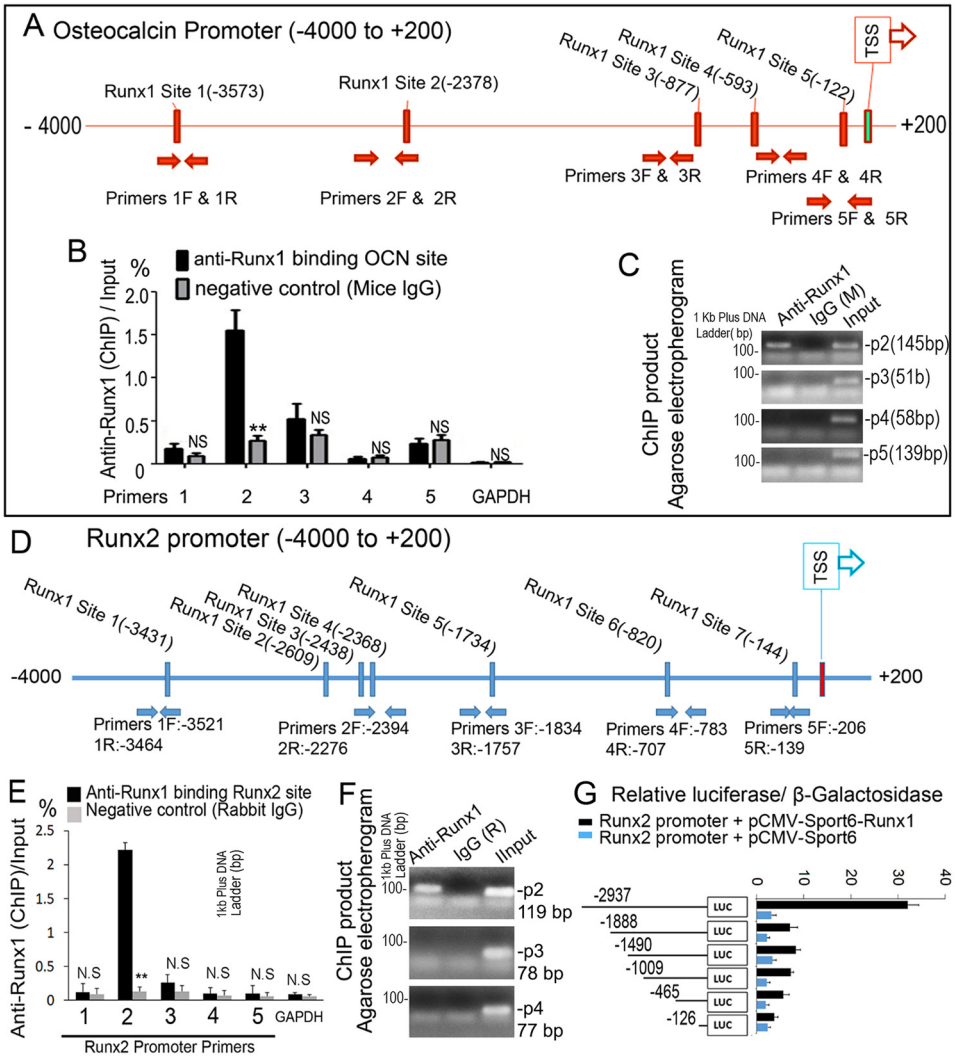

Figure 7. RUNX1 regulates *Runx2* expression by directly associating with its promoters. *A,* schematic display of the *Ocn* (–4000/+200) promoter region: *TSS*, predicted RUNX1-binding sites, and ChIP primers positions. *B,* ChIP analysis of RUNX1 binding to the *Ocn* promoter in WT calvaria-derived osteoblasts using primers as indicated on the *x* axis. Results are presented as ChIP/Input. *C,* agarose gel image using ChIP qPCR products in *B*. *D,* schematic display of *Runx2* (–4000/+200) promoter region: TSS, predicted RUNX1-binding sites, and ChIP primers positions. *E,* ChIP analysis of RUNX1 binding to the *Runx2* promoter in WT calvaria-derived osteoblast using primers as indicated on the *x* axis. Results are presented as ChIP/Input. *F,* agarose gel image using ChIP qPCR products in *E*. *G, Runx2* promoter fragments were inserted into pG13-basic vector. C3H10T1/2 cells were transfected with pG13-Runx2 –126 bp, –465 bp, –1009 bp, –1409 bp, –1888 bp, and –2937 bp. Luciferase was detected at 48 h post-transfection and normalized to β-gal activity. Results are presented as mean ± S.D. with $n = 3$. *N.S.*, not significant; *, $p < 0.05$; **, $p < 0.01$.

regulating *Rankl* expression (38). Although it was previously believed that OSX functions exclusively as an osteoblast-specific transcription factor, our results and that of others (39–41) demonstrate that *Osx* also plays a role in postnatal chondrogenesis. Previous reports have demonstrated that *Osx* couples chondrogenesis and osteogenesis in postnatal condylar growth, and is essential for the coupling of terminal cartilage differentiation (39). Furthermore, Osx-Cre also targets olfactory glomerular cells and a subset of the gastric and intestinal epithelium in postnatal mice (40). Notably, Cheng *et al.* (41) demonstrated that haploinsufficiency of OSX in chondrocytes impairs skeletal growth in mice. Previous reports demonstrate that the Osx-Cre transgene itself has no effect on the trabecular bone parameters and minimal effect on the cortical parameters for 1-month–old mice, and as the mature mice, they display comparable cortical and trabecular bone parameters compared with the control mice (22, 42). At 6 weeks of age, Osx-Cre mice display reduced body weight and delayed cortical bone expansion and accrual, however, the delayed weight gain and cortical growth bone of Osx-Cre mice is overcome by 12 weeks of age, with no differences between Osx-Cre and WT mice (43). Thus, the phenotype observed in the *Runx1*$^{f/f}$*Osx-Cre* mice was due to the deletion of *Runx1*, and not due to the Osx-Cre transgene itself.

Our *in vitro* mechanistic studies demonstrate that Runx1 conditional deletion in osteoblast precursors and differentiating chondrocytes has significant effects on genes critical for skeletal development such as *Runx2*, *Osx*, *Atf4*, and *Ocn*. These findings suggest that RUNX1 plays an indispensable role in postnatal skeletal development and bone homeostasis by up-regulating the expression of *Runx2* and multiple bone genes. Our study shows that RUNX1 associates with the promoter

regions of *Runx2* and *Ocn* and highly up-regulates the expression of *Runx2* at the transcriptional regulation level as shown by ChIP assay, qPCR analysis, and promoter reporter assay. Although we found multiple binding sites for RUNX1 on the *Runx2* promoter, we found that RUNX1 potentially binds to the *Runx2* promoter around binding site 4. Previous reports have shown that RUNX1 mediates epigenetic regulation to inhibit or facilitate multiple regulatory regions in the target genes (44–46). RUNX1 has been shown to interact with histone acetyltransferases, as well as components of the histone deacetylase complex (46). Thus, the interaction of RUNX1 with histone acetyltransferases acetylates chromatin-associated histones, which lead to chromatin conformational changes and transcriptional activation, could be responsible for the high binding efficiency of RUNX1 on the *Runx2* promoter at binding site 4. However, the landscape of epigenetic alterations in many cell types is distinctively complex, thus future research is warranted to fully explore whether and how RUNX1 leads to epigenetic changes at genes central to osteoblastic lineage commitment.

Because *Runx2* exhibits high homology with *Runx1*, it has been suspected that *Runx1* may be responsible for some cases of CCD. Although no *Runx1* mutation has yet been identified in classical CCD patients, our *Runx1$^{f/f}$Osx-Cre* mouse models support the notion that search genetic alterations in the *Runx1* gene may be responsible for CCD in those patients with no *Runx2* mutation. Our results are in agreement with that of previous studies reporting that Runx2 deficiency causes an arrest in clavicular development (47). These findings provide great insight into the pathogenesis of CCD and the role of *Runx1* in both postnatal skeletal and tooth development.

Overall, our genetic dissection approach revealed that RUNX1 plays an indispensable role in postnatal skeletal development and bone homeostasis by up-regulating the expression of *Runx2* and multiple bone genes. Our study of *Runx1* in the osteoblast lineage has demonstrated that *Runx1* is required to promote chondrocyte and osteoblast differentiation to maintain bone homeostasis. Targeting RUNX1, a regulator of both *Runx2* and bone genes, could facilitate the design of safer and novel therapeutic approaches for osteoporosis. Taken together, this work provides important insights into the role of RUNX1 in bone formation and the mechanisms underlying how RUNX1 maintains bone homeostasis. The insights resulting from this study may assist in the development of novel treatments for osteoporosis and other osteolytic diseases.

Experimental procedures

For more detailed descriptions, please refer to the Supporting Materials and Methods. For primer sequences please refer to Tables S1–S3.

Generation of Runx1$^{f/f}$Osx-Cre mice

All animal experimentation was carried out according to the legal requirements of the Association for Assessment and Accreditation of the Laboratory Animal Care International and the University of Alabama at Birmingham Institutional Animal Care and Use Committee. Jackson Laboratory, strain name B6.129P2-Runx1tm1Tani/J, JAX No. 008772, were crossed with skeletal tissue cell (including osteoblast precursors, osteoblasts, chondrocytes, and odontoblasts)-specific *Osx-Cre* mice (19) (*Tg(Sp7-tTA,tetO-EGFP/cre)1Amc*, Mouse Genome Informatics) Their progeny were crossed with *Runx1$^{f/f}$* mice to obtain *Runx1$^{f/f}$Osx-Cre* mice. In our study, we only use one copy of *Osx-Cre* (*Runx1$^{f/f}$ Osx-Cre/+*) in the CKO mutation. *Osx-Cre* mice had no detectable bone phenotype and served as control groups along with *Runx1$^{f/f}$* mice. Mice were bred in-house and euthanized by CO_2 asphyxiation. All mice were maintained under a 12-h light–dark cycle with *ad libitum* access to regular food and water at the University of Alabama Animal Facility. Both male and female mice of each strain were randomly selected into groups of five animals each. The investigators were not blinded during allocation, animal handling, and end point measurements. Genotyping by PCR was carried out as described (48).

Histomorphometric analysis

Histomorphometric samples were processed as un-decalcified hard-tissue sections as described (49, 50). Bone parameters were quantified via 6-μm sections obtained from mice.

Primary cell culture

Calvarial cells were isolated from newborn mice and seeded in cell culture dishes at a density of 3×10^3 cells/cm^2 as described (51). After growing to confluence, cells were induced to differentiate into osteoblasts using osteogenic medium supplemented with 10% (v/v) FBS, 50 μg/ml of L-ascorbic acid (Sigma, A4544), and 5 mM β-glycerolphosphate (Sigma, G9891). Osteoblastogenesis was analyzed by ALP staining according to the manufacturer's manual (Sigma, A2356) on day 14. Osteoblast mineralization was examined by Von Kossa staining on day 21.

ChIP

Cells were derived from calvaria of newborn WT mice, and ChIP was performed as described (52). After immunoprecipitation using monoclonal anti-Runx1 antibody (ab23980; Abcam) and DNA extraction, quantitative PCR was performed using the primers in the promoter region of the mouse gene *Runx2*.

RNA-Sequencing analysis

Total mRNA was isolated using TRIzol reagent (Invitrogen Corp.) from the osteoblasts that were cultured for 14 days in osteoblasts differentiation medium following the manufacturer's protocol and submitted to Admera Health (South Plainsfield, NJ) who assessed sample quality with the Agilent Bioanalyzer and prepared the library using the NEBnext Ultra RNA-Poly(A) kit. Libraries were analyzed using Illumina next generation sequencing and relative quantification was provided by Admera Health.

Promoter analyses

Runx2 promoter sequences were analyzed for putative RUNX-binding sites with PROMO3.0 (RRID:SCR_016926) using version 8.3 of the TRANSFAC database. The promoter region (−) and (+) of the mouse *Runx2* gene was amplified by PCR using *Runx2* Bac clone (catalog No. CH29-571B2; CHORI). Then the promoter regions were inserted into the pGL3-basic vector to construct the pGL3-Runx2 promoter fragments. The insertions of the constructs were confirmed by sequencing. C3H10T1/2 cells were cultured in 24-well–plates, and were transiently transfected with a DNA mixture containing the pGL3-Runx2 construct (0.3 μg) and β-Gal-expressing plasmids (0.06 μg), with or without *Runx1* expressing vector (pCMV-Sport6-Runx1, 0.3 μg) using Lipofectamine and Plus reagents. Luciferase was detected using Glo Luciferase Assay System (Promega) 48 h post-transfection as described (52). The β-Gal activity of the cell lysates was analyzed using β-Galactosidase Enzyme Assay System (E2000; Promega). The level of luciferase activity was normalized to the level of β-Gal activity.

Statistical analysis

All data are presented as the mean ± S.D. ($n \geqq 6$). Statistical significance was assessed using Student's *t test*. p values <0.05 were considered significant. Data are expressed as mean ± S.D., $n \geqq 6$, *, $p < 0.05$; **, $p < 0.01$; ***, $p < 0.001$. The results are representative of at least four individual experiments. The analyses of the data were performed with the SPSS 16.0 software (SPSS Incorporation, Chicago, IL, USA).

Data availability

The RNA-Seq data are available upon request from Yi-Ping Li, Department of Pathology, University of Alabama at Birmingham, E-mail: yipingli@uabmc.edu. All other data are contained within the manuscript.

Acknowledgments—We thank Abigail McVicar for excellent assistance with the manuscript, and Matthew McConnell for bioinformatics analysis assistance. We appreciate the assistance provided by the Center for Metabolic Bone Disease at the University of Alabama at Birmingham supported by Grant P30 AR046031. We are also grateful for the assistance from the Small Animal Phenotyping Core, Metabolism Core, and Neuroscience Molecular Detection Core Laboratory at the University of Alabama at Birmingham supported by Grant P30 NS0474666.

Author contributions—J. T., J. X., W. C., C. T., J. W., Y. W., X.-d. Z., H.-D. Z., and Y.-P. L. data curation; J. T., J. X., W. C., C. T., J. W., Y. W., X.-d. Z., H.-D. Z., and Y.-P. L. formal analysis; J. T., J. X., W. C., C. T., J. W., Y. W., X.-d. Z., H.-D. Z., and Y.-P. L. investigation; J. T., W. C., H.-D. Z., and Y.-P. L methodology; J. T., W. C., X.-d. Z., H-D. Z., and Y-P. L. writing-original draft; J. T., W. C., C. T., X.-d. Z., H.-D. Z., and Y.-P. L. writing-review and editing; J. X., W. C., C. T., Y. W., H.-D. Z., and Y.-P. L. visualization; W. C. and Y.-P. L. conceptualization; W. C., H.-D. Z., and Y.-P. L. supervision; W. C. and Y.-P. L. funding acquisition; W. C. and Y.-P. L. validation; Y.-P. L. resources; Y.-P. L. project administration.

Funding and additional information—This work was supported by National Institutes of Health Grants AR-075735, DE-028264 (to Y.-P. L.), AR-070135 and AG-056438 (to W. C.), and China Scholarship Council Grant 201606370184 (to J. T.). The content is solely the responsibility of the authors and does not necessarily represent the official views of the National Institutes of Health.

Conflict of interest—The authors declare that they have no conflicts of interest with the contents of this article.

Abbreviations—The abbreviations used are: Runx1, Runt-related transcription factor 1; Osx, Osterix; Runx2, Runt-related transcription factor 2; Sox9, SRY-related high-mobility group-box gene 9; Ihh, Indian hedgehog; PTC, Patched; Ocn, osteocalcin; Atf4, activating transcription factor 4; qPCR, quantitative polymerase chain reaction; IHC, immunohistochemical; μCT, micro-computed tomography; H&E, hematoxylin and eosin; ALP, alkaline phosphatase; TRAP, tartrate-resistant acid phosphatase; CKO, conditional knockout; PCNA, proliferating cell nuclear antigen; IF, immunofluorescent; CCD, cleidocranial dysplasia; GAPDH, glyceraldehyde-3-phosphate dehydrogenase; DAPI, 4′,6-diamidino-2-phenylindole.

References

1. Nam, M., Huh, J. E., Kim, M. S., Ryu, D. H., Park, J., Kim, H. S., Lee, S. Y., and Hwang, G. S. (2018) Metabolic alterations in the bone tissues of aged osteoporotic mice. *Sci. Rep.* **8,** 8127 CrossRef Medline
2. Brommage, R., and Ohlsson, C. (2018) Translational studies provide insights for the etiology and treatment of cortical bone osteoporosis. *Best Pract. Res. Clin. Endocrinol. Metab.* **32,** 329–340 CrossRef Medline
3. Miyamoto, T. (2018) Homeostasis and disorder of musculoskeletal system: pathogenesis of musculoskeletal diseases and strategies for their treatment. *Clin. Calcium* **28,** 301–305 Medline
4. Komori, T. (2005) Regulation of skeletal development by the Runx family of transcription factors. *J. Cell. Biochem.* **95,** 445–453 CrossRef Medline
5. Okuda, T., Nishimura, M., Nakao, M., and Fujita, Y. (2001) RUNX1/AML1: a central player in hematopoiesis. *Int. J. Hematol.* **74,** 252–257 CrossRef Medline
6. Chen, C. L., Broom, D. C., Liu, Y., de Nooij, J. C., Li, Z., Cen, C., Samad, O. A., Jessell, T. M., Woolf, C. J., and Ma, Q. (2006) Runx1 determines nociceptive sensory neuron phenotype and is required for thermal and neuropathic pain. *Neuron* **49,** 365–377 CrossRef Medline
7. Kimura, A., Inose, H., Yano, F., Fujita, K., Ikeda, T., Sato, S., Iwasaki, M., Jinno, T., Ae, K., Fukumoto, S., Takeuchi, Y., Itoh, H., Imamura, T., Kawaguchi, H., Chung, U. I., *et al.* (2010) Runx1 and Runx2 cooperate during sternal morphogenesis. *Development* **137,** 1159–1167 CrossRef Medline
8. Liakhovitskaia, A., Lana-Elola, E., Stamateris, E., Rice, D. P., van 't Hof, R. J., and Medvinsky, A. (2010) The essential requirement for Runx1 in the development of the sternum. *Dev. Biol.* **340,** 539–546 CrossRef Medline
9. Soung do, Y., Talebian, L., Matheny, C. J., Guzzo, R., Speck, M. E., Lieberman, J. R., Speck, N. A., and Drissi, H. (2012) Runx1 dose-dependently regulates endochondral ossification during skeletal development and fracture healing. *J. Bone Miner. Res.* **27,** 1585–1597 CrossRef Medline
10. Wang, Y., Belflower, R. M., Dong, Y. F., Schwarz, E. M., O'Keefe, R. J., and Drissi, H. (2005) Runx1/AML1/Cbfa2 mediates onset of mesenchymal cell differentiation toward chondrogenesis. *J. Bone Miner. Res.* **20,** 1624–1636 CrossRef Medline
11. Lian, J. B., Balint, E., Javed, A., Drissi, H., Vitti, R., Quinlan, E. J., Zhang, L., Van Wijnen, A. J., Stein, J. L., Speck, N., and Stein, G. S. (2003) Runx1/AML1 hematopoietic transcription factor contributes to skeletal development *in vivo*. *J. Cell. Physiol.* **196,** 301–311 CrossRef Medline

12. Ducy, P., Zhang, R., Geoffroy, V., Ridall, A. L., and Karsenty, G. (1997) Osf2/Cbfa1: a transcriptional activator of osteoblast differentiation. *Cell* **89,** 747–754 CrossRef Medline
13. Komori, T., Yagi, H., Nomura, S., Yamaguchi, A., Sasaki, K., Deguchi, K., Shimizu, Y., Bronson, R. T., Gao, Y. H., Inada, M., Sato, M., Okamoto, R., Kitamura, Y., Yoshiki, S., and Kishimoto, T. (1997) Targeted disruption of Cbfa1 results in a complete lack of bone formation owing to maturational arrest of osteoblasts. *Cell* **89,** 755–764 CrossRef
14. Otto, F., Thornell, A. P., Crompton, T., Denzel, A., Gilmour, K. C., Rosewell, I. R., Stamp, G. W., Beddington, R. S., Mundlos, S., Olsen, B. R., Selby, P. B., and Owen, M. J. (1997) *Cbfa1*, a candidate gene for cleidocranial dysplasia syndrome, is essential for osteoblast differentiation and bone development. *Cell* **89,** 765–771 CrossRef Medline
15. Soltanoff, C. S., Chen, W., Yang, S., and Li, Y.-P. (2009) Signaling networks that control the lineage commitment and differentiation of bone cells. *Crit. Rev. Eukaryot. Gene Expr.* **19,** 1–46 CrossRef Medline
16. Komori, T. (2018) Runx2, an inducer of osteoblast and chondrocyte differentiation. *Histochem. Cell Biol.* **149,** 313–323 CrossRef Medline
17. Geoffroy, V., Kneissel, M., Fournier, B., Boyde, A., and Matthias, P. (2002) High bone resorption in adult aging transgenic mice overexpressing cbfa1/runx2 in cells of the osteoblastic lineage. *Mol. Cell Biol.* **22,** 6222–6233 CrossRef Medline
18. Smith, N., Dong, Y., Lian, J. B., Pratap, J., Kingsley, P. D., van Wijnen, A. J., Stein, J. L., Schwarz, E. M., O'Keefe, R. J., Stein, G. S., and Drissi, M. H. (2005) Overlapping expression of Runx1(Cbfa2) and Runx2(Cbfa1) transcription factors supports cooperative induction of skeletal development. *J. Cell. Physiol.* **203,** 133–143 CrossRef Medline
19. Rodda, S. J., and McMahon, A. P. (2006) Distinct roles for Hedgehog and canonical Wnt signaling in specification, differentiation and maintenance of osteoblast progenitors. *Development* **133,** 3231–3244 CrossRef Medline
20. Chen, S., Gluhak-Heinrich, J., Wang, Y. H., Wu, Y. M., Chuang, H. H., Chen, L., Yuan, G. H., Dong, J., Gay, I., and MacDougall, M. (2009) Runx2, osx, and dspp in tooth development. *J. Dent. Res.* **88,** 904–909 CrossRef Medline
21. Huang, W., and Olsen, B. R. (2015) Skeletal defects in Osterix-Cre transgenic mice. *Transgenic Res.* **24,** 167–172 CrossRef Medline
22. Wang, L., Mishina, Y., and Liu, F. (2015) Osterix-Cre transgene causes craniofacial bone development defect. *Calcif. Tissue Int.* **96,** 129–137 CrossRef Medline
23. Provot, S., and Schipani, E. (2005) Molecular mechanisms of endochondral bone development. *Biochem. Biophys. Res. Commun.* **328,** 658–665 CrossRef Medline
24. Long, F., Zhang, X. M., Karp, S., Yang, Y., and McMahon, A. P. (2001) Genetic manipulation of hedgehog signaling in the endochondral skeleton reveals a direct role in the regulation of chondrocyte proliferation. *Development* **128,** 5099–5108 Medline
25. Berendsen, A. D., and Olsen, B. R. (2015) Bone development. *Bone* **80,** 14–18 CrossRef Medline
26. Wang, J., Wang, X., Holz, J. D., Rutkowski, T., Wang, Y., Zhu, Z., and Dong, Y. (2013) Runx1 is critical for PTH-induced onset of mesenchymal progenitor cell chondrogenic differentiation. *PLoS ONE* **8,** e74255 CrossRef Medline
27. Myllyharju, J. (2014) Extracellular matrix and developing growth plate. *Curr. Osteoporos. Rep.* **12,** 439–445 CrossRef Medline
28. Johnson, K., Zhu, S., Tremblay, M. S., Payette, J. N., Wang, J., Bouchez, L. C., Meeusen, S., Althage, A., Cho, C. Y., Wu, X., and Schultz, P. G. (2012) A stem cell-based approach to cartilage repair. *Science* **336,** 717–721 CrossRef Medline
29. Wu, M., Li, C., Zhu, G., Wang, Y., Jules, J., Lu, Y., McConnell, M., Wang, Y. J., Shao, J. Z., Li, Y. P., and Chen, W. (2014) Deletion of core-binding factor beta (Cbfβ) in mesenchymal progenitor cells provides new insights into Cbfβ/Runxs complex function in cartilage and bone development. *Bone* **65,** 49–59 CrossRef Medline
30. Foster, J. W., Dominguez-Steglich, M. A., Guioli, S., Kwok, C., Weller, P. A., Stevanovic, M., Weissenbach, J., Mansour, S., Young, I. D., and Goodfellow, P. N. and (1994) Campomelic dysplasia and autosomal sex reversal caused by mutations in an SRY-related gene. *Nature* **372,** 525–530 CrossRef Medline
31. Wagner, T., Wirth, J., Meyer, J., Zabel, B., Held, M., Zimmer, J., Pasantes, J., Bricarelli, F. D., Keutel, J., Hustert, E., Wolf, U., Tommerup, N., Schempp, W., and Scherer, G. (1994) Autosomal sex reversal and campomelic dysplasia are caused by mutations in and around the SRY-related gene SOX9. *Cell* **79,** 1111–1120 CrossRef Medline
32. Barna, M., and Niswander, L. (2007) Visualization of cartilage formation: insight into cellular properties of skeletal progenitors and chondrodysplasia syndromes. *Dev. Cell* **12,** 931–941 CrossRef Medline
33. Long, F., and Ornitz, D. M. (2013) Development of the endochondral skeleton. *Cold Spring Harb. Perspect. Biol.* **5,** a008334 CrossRef Medline
34. Kronenberg, H. M. (2003) Developmental regulation of the growth plate. *Nature* **423,** 332–336 CrossRef Medline
35. Maeda, Y., Nakamura, E., Nguyen, M. T., Suva, L. J., Swain, F. L., Razzaque, M. S., Mackem, S., and Lanske, B. (2007) Indian Hedgehog produced by postnatal chondrocytes is essential for maintaining a growth plate and trabecular bone. *Proc. Natl. Acad. Sci. U.S.A.* **104,** 6382–6387 CrossRef Medline
36. Long, F., Chung, U. I., Ohba, S., McMahon, J., Kronenberg, H. M., and McMahon, A. P. (2004) Ihh signaling is directly required for the osteoblast lineage in the endochondral skeleton. *Development (Cambridge, Eng.)* **131,** 1309–1318 CrossRef Medline
37. Karp, S. J., Schipani, E., St-Jacques, B., Hunzelman, J., Kronenberg, H., and McMahon, A. P. (2000) Indian hedgehog coordinates endochondral bone growth and morphogenesis via parathyroid hormone related-protein-dependent and -independent pathways. *Development (Cambridge, Eng.)* **127,** 543–548 Medline
38. Mak, K. K., Bi, Y., Wan, C., Chuang, P. T., Clemens, T., Young, M., and Yang, Y. (2008) Hedgehog signaling in mature osteoblasts regulates bone formation and resorption by controlling PTHrP and RANKL expression. *Dev. Cell* **14,** 674–688 CrossRef Medline
39. Jing, J., Hinton, R. J., Jing, Y., Liu, Y., Zhou, X., and Feng, J. Q. (2014) Osterix couples chondrogenesis and osteogenesis in post-natal condylar growth. *J. Dental Res.* **93,** 1014–1021 CrossRef Medline
40. Chen, J., Shi, Y., Regan, J., Karuppaiah, K., Ornitz, D. M., and Long, F. (2014) Osx-Cre targets multiple cell types besides osteoblast lineage in postnatal mice. *PLoS ONE* **9,** e85161 CrossRef Medline
41. Cheng, S., Xing, W., Zhou, X., and Mohan, S. (2013) Haploinsufficiency of osterix in chondrocytes impairs skeletal growth in mice. *Physiol. Genomics* **45,** 917–923 CrossRef
42. Liu, F., Fang, F., Yuan, H., Yang, D., Chen, Y., Williams, L., Goldstein, S. A., Krebsbach, P. H., and Guan, J.-L. (2013) Suppression of autophagy by FIP200 deletion leads to osteopenia in mice through the inhibition of osteoblast terminal differentiation. *J. Bone Miner. Res.* **28,** 2414–2430 CrossRef Medline
43. Davey, R. A., Clarke, M. V., Sastra, S., Skinner, J. P., Chiang, C., Anderson, P. H., and Zajac, J. D. (2012) Decreased body weight in young Osterix-Cre transgenic mice results in delayed cortical bone expansion and accrual. *Transgenic Res.* **21,** 885–893 CrossRef
44. Kitabayashi, I., Aikawa, Y., Nguyen, L. A., Yokoyama, A., and Ohki, M. (2001) Activation of AML1-mediated transcription by MOZ and inhibition by the MOZ-CBP fusion protein. *EMBO J.* **20,** 7184–7196 CrossRef Medline
45. Allende-Vega, N., Dayal, S., Agarwala, U., Sparks, A., Bourdon, J. C., and Saville, M. K. (2013) p53 is activated in response to disruption of the pre-mRNA splicing machinery. *Oncogene* **32,** 1–14 CrossRef Medline
46. Koh, C. P., Wang, C. Q., Ng, C. E., Ito, Y., Araki, M., Tergaonkar, V., Huang, G., and Osato, M. (2013) RUNX1 meets MLL: epigenetic regulation of hematopoiesis by two leukemia genes. *Leukemia* **27,** 1793–1802 CrossRef Medline
47. Cohen, M. M. Jr (2013) Biology of RUNX2 and cleidocranial dysplasia. *J. Craniofacial Surg.* **24,** 130–133 CrossRef Medline
48. Growney, J. D., Shigematsu, H., Li, Z., Lee, B. H., Adelsperger, J., Rowan, R., Curley, D. P., Kutok, J. L., Akashi, K., Williams, I. R., Speck, N. A., and Gilliland, D. G. (2005) Loss of Runx1 perturbs adult hematopoiesis and is associated with a myeloproliferative phenotype. *Blood* **106,** 494–504 CrossRef Medline
49. Chen, W., Yang, S., Abe, Y., Li, M., Wang, Y., Shao, J., Li, E., and Li, Y. P. (2007) Novel pycnodysostosis mouse model uncovers cathepsin K

function as a potential regulator of osteoclast apoptosis and senescence. *Hum. Mol. Genet.* **16,** 410–423 CrossRef Medline

50. Yang, S., and Li, Y. P. (2007) RGS10-null mutation impairs osteoclast differentiation resulting from the loss of $[Ca^{2+}]i$ oscillation regulation. *Genes Dev.* **21,** 1803–1816 CrossRef Medline
51. Pockwinse, S. M., Wilming, L. G., Conlon, D. M., Stein, G. S., and Lian, J. B. (1992) Expression of cell growth and bone specific genes at single cell resolution during development of bone tissue-like organization in primary osteoblast cultures. *J. Cell. Biochem.* **49,** 310–323 CrossRef Medline
52. Chen, W., Ma, J., Zhu, G., Jules, J., Wu, M., McConnell, M., Tian, F., Paulson, C., Zhou, X., Wang, L., and Li, Y. P. (2014) Cbfβ deletion in mice recapitulates cleidocranial dysplasia and reveals multiple functions of Cbfβ required for skeletal development. *Proc. Natl. Acad. Sci. U.S.A.* **111,** 8482–8487 CrossRef Medline

Runt-related transcription factor 1 is required for murine osteoblast differentiation and bone formation

Jun Tang, Jing Xie, Wei Chen, Chenyi Tang, Jinjin Wu, Yiping Wang, Xue-Dong Zhou, Hou-De Zhou and Yi-Ping Li

J. Biol. Chem. 2020, 295:11669-11681.
doi: 10.1074/jbc.RA119.007896 originally published online June 22, 2020

Runt-Related Transcription Factor 1 is required for murine osteoblast differentiation and bone formation

Jun Tang[1, 2, #], Jing Xie[2,3, #], Wei Chen[2*], Chenyi Tang[2], Jinjin Wu[2], Yiping Wang[2], Xue-Dong Zhou[3], Hou-De Zhou[1*], and Yi-Ping Li[2*]

Supporting Materials included:

Supplemental Figures and Figure Legends

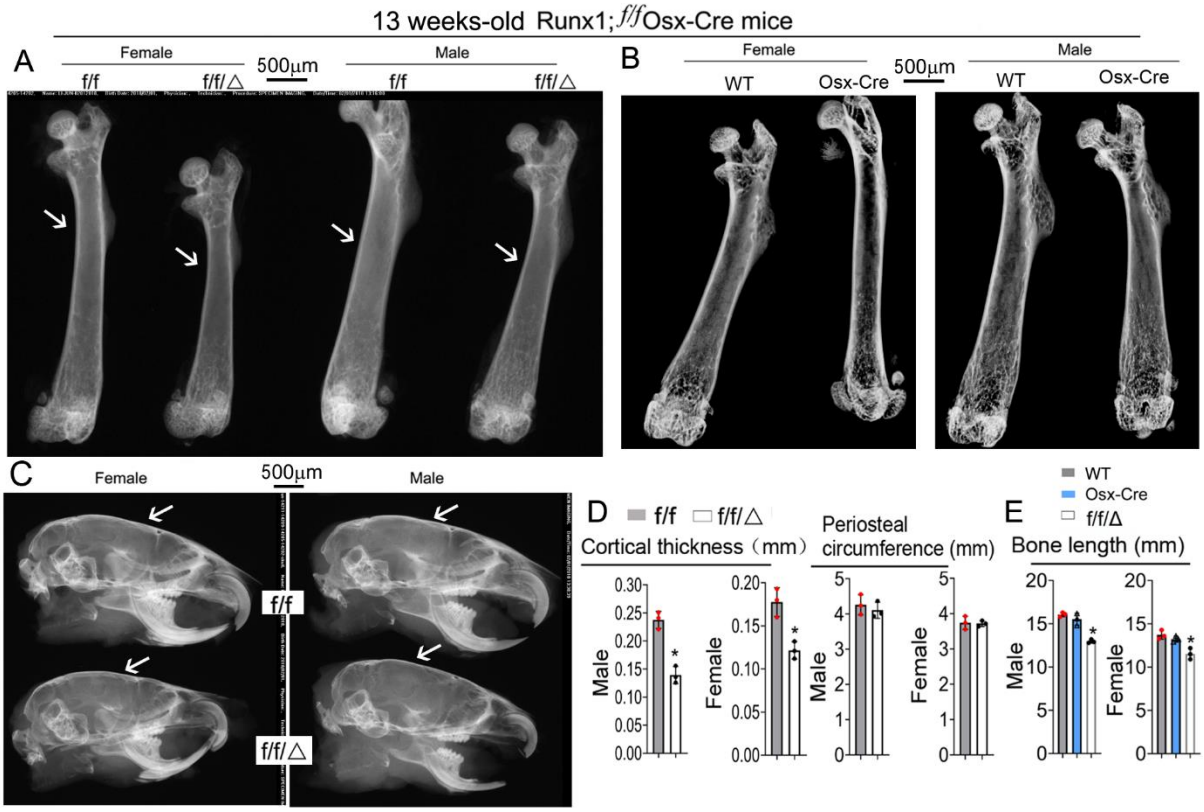

Supplemental Figure 1. *Runx1$^{f/f}$Osx-Cre* mice but not Osx-cre mice have decreased bone mineralization at 13 weeks old. (A) X-ray analysis of 13-week-old female and male Runx1$^{f/f}$*Osx-Cre* (f/f/Δ), and wild-type (f/f) femurs. (B) X-ray analysis of 13-week-old female and male wild-type (f/f) and *Osx-Cre* femurs. (C) X-ray analysis of 13-week-old female and male Runx1$^{f/f}$ *Osx-Cre* (f/f/Δ), and wild-type (f/f) skulls. (D) The cortical thickness and periosteal circumference of female and male Runx1$^{f/f}$*Osx-Cre* (f/f/Δ), and wild-type (f/f) femurs, and the femur length of the female and male Runx1$^{f/f}$*Osx-Cre* (f/f/Δ), *Osx-Cre* and wild-type (f/f). White arrows indicate reduced ossification. Results are presented as mean ± SD with n=6 in each group. *p<0.05.

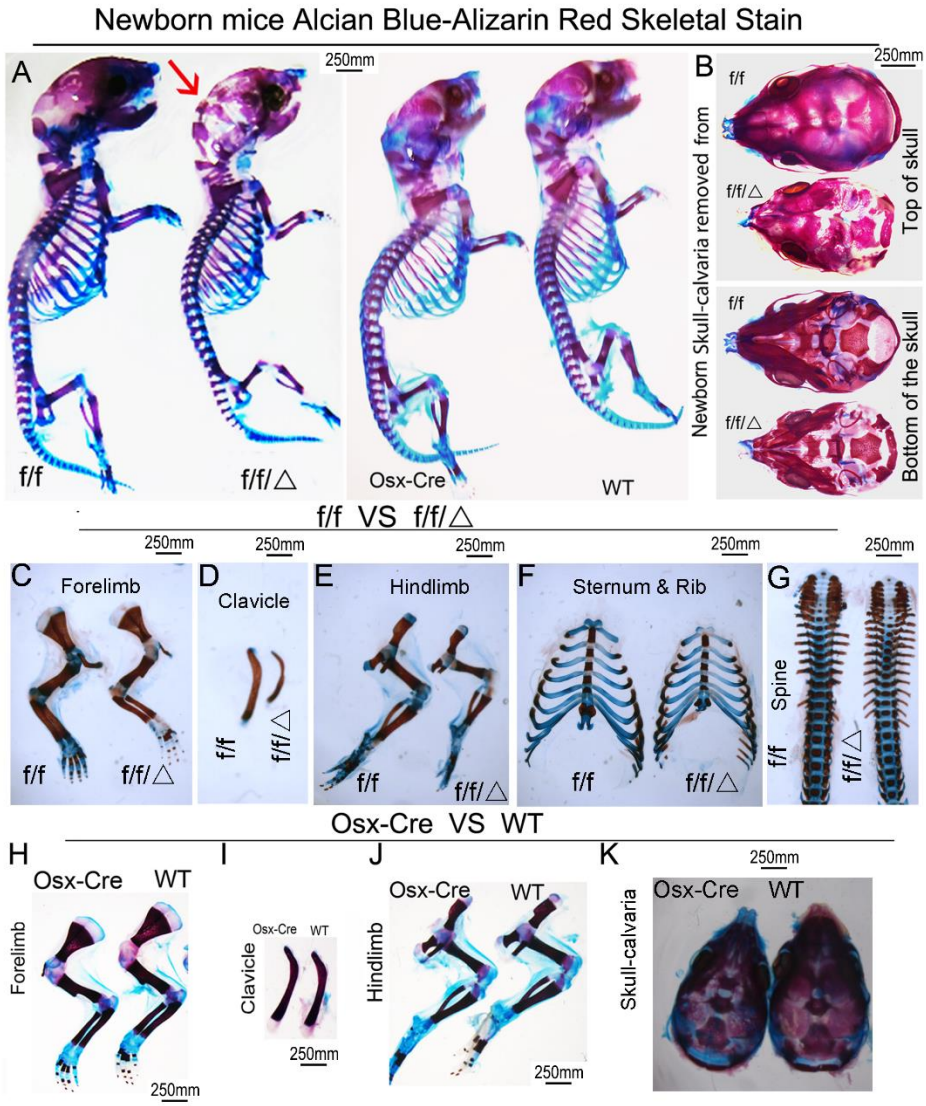

Supplemental Figure 2. *Runx1* depletion in osteoblasts results in decreased ossification. (A) Whole-mount Alizarin red and Alcian blue staining of P0 *Runx1*$^{f/f}$*Osx-Cre* (f/f/Δ), wild-type (f/f), and Osx-cre mice skeletons. (B) Whole-mount Alizarin red and Alcian blue staining of P0 *Runx1*$^{f/f}$*Osx-Cre* (f/f/Δ) and wild-type (f/f) mice cranium (top) and cranial base (bottom). n=3. (C-G) Whole-mount Alizarin red and Alcian blue staining of P0 *Runx1*$^{f/f}$*Osx-Cre* (f/f/Δ) and wild-type (f/f) mice (C) forelimbs, (D) clavicles, (E) hindlimbs, (F) sternum and ribs, and (G) vertebrae. Whole-mount Alizarin red and Alcian blue staining of P0 *Osx-cre* and WT mice (H) forelimbs, (I) clavicles, (J) hindlimbs, and (K) skulls. n=10.

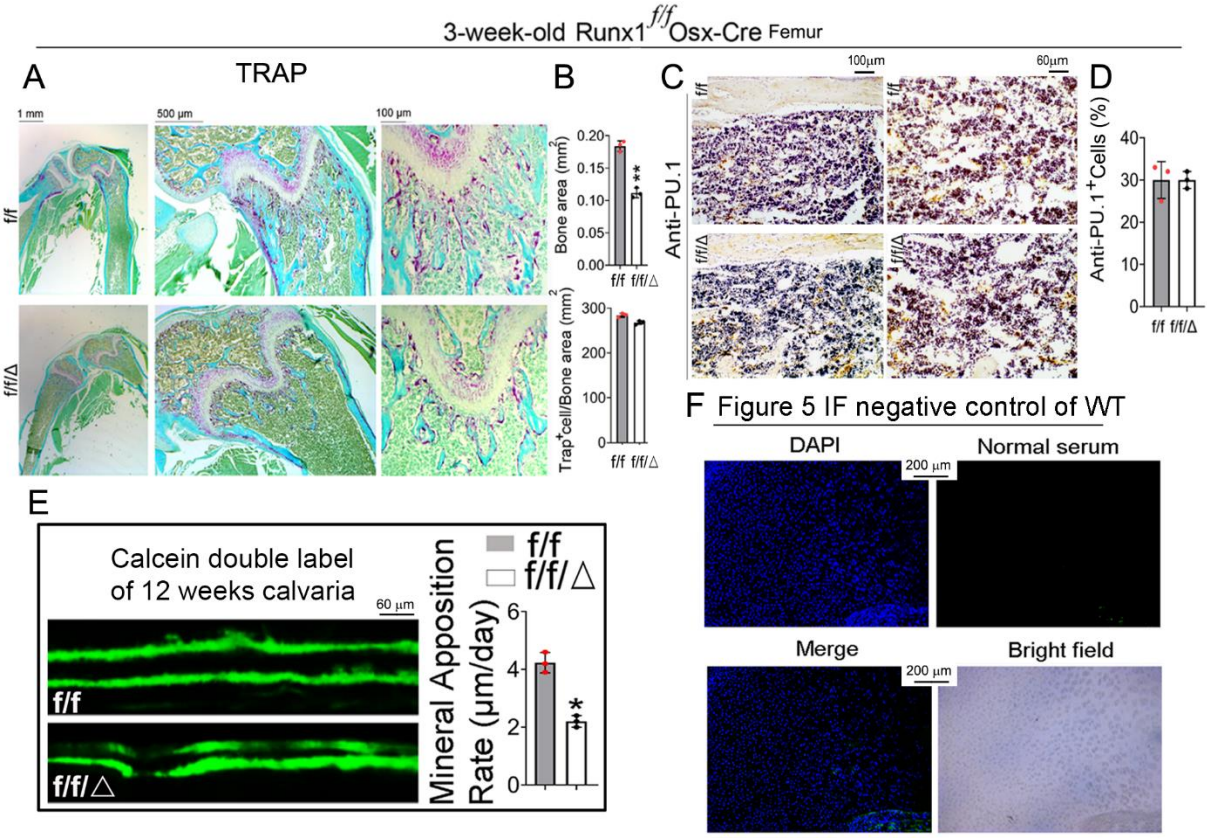

Supplemental Figure 3. Osteoclast formation is not affected in 3-week-old *Runx1$^{f/f}$Osx-Cre* femurs. (A) 3-week-old *Runx1$^{f/f}$Osx-Cre* (f/f/Δ) and wild-type (f/f) mice femurs were stained with TRAP stain to detect osteoclast formation. (B) Quantification of A. (C) IHC staining PU.1 antibody of femur paraffin sections from 3-week-old Runx1f/fOsx-Cre (f/f/Δ), and wild-type (f/f) mice. (D) Quantification of C. (E) Calcein double label of 3-month-old mice and Mineral apposition rate. (F) Immunofluorescence (IF) stain of Anti-Sox9 negative control from Figure 5A. Results are expressed as mean ± SD. n=3 in each group. N.S, not significant; ***p*<0.01.

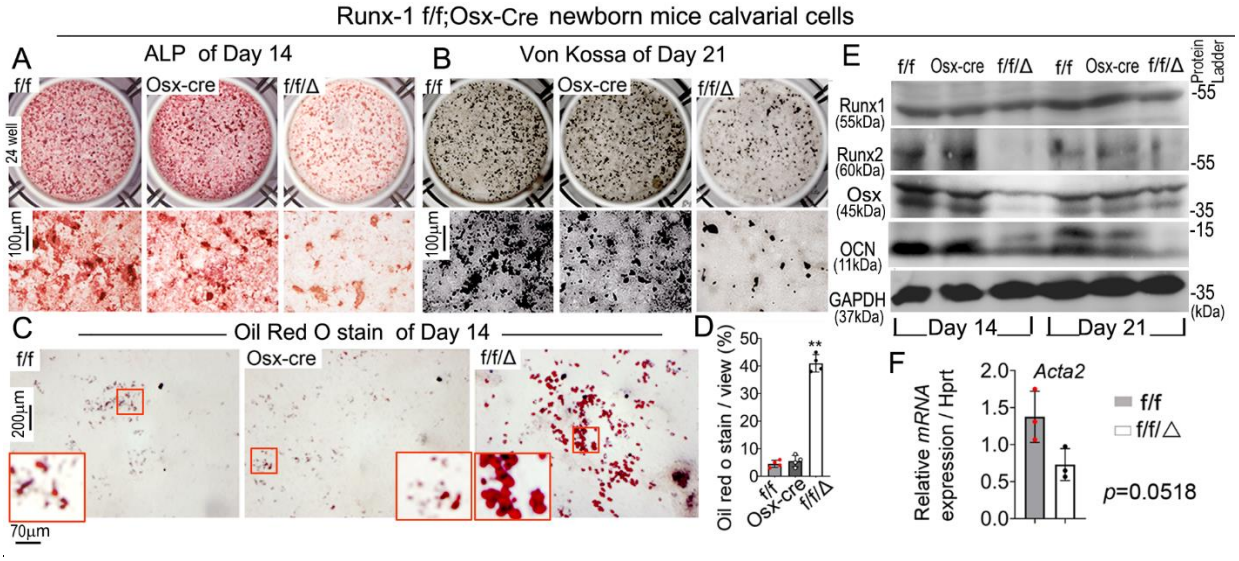

Supplemental Figure 4. Runx1-deficiency in primary calvarial cells cultured from *Runx1$^{f/f}$Osx-Cre* mice inhibits osteoblastogenesis and promotes adipogenesis. (A-C) Calvarial cells from *Runx1$^{f/f}$Osx-Cre* (f/f/Δ), *Osx-Cre*, and wild-type (f/f) newborn mice were cultured in osteogenic medium for 14 days and 21 days, followed by ALP, Von Kossa stain, or Oil red O stain. (D) Quantification of C. (E) Protein levels of Runx1, Runx2, Osx, and Ocn were analyzed by Western blot analysis on day 7 and day 14. GAPDH is shown as a control. (F) qPCR analysis of mRNA expression levels of *Acta2* in calvaria-derived osteoblasts from *Runx1$^{f/f}$Osx-Cre* (f/f/Δ) and wild-type (f/f) mice. $^{**}p<0.01$.

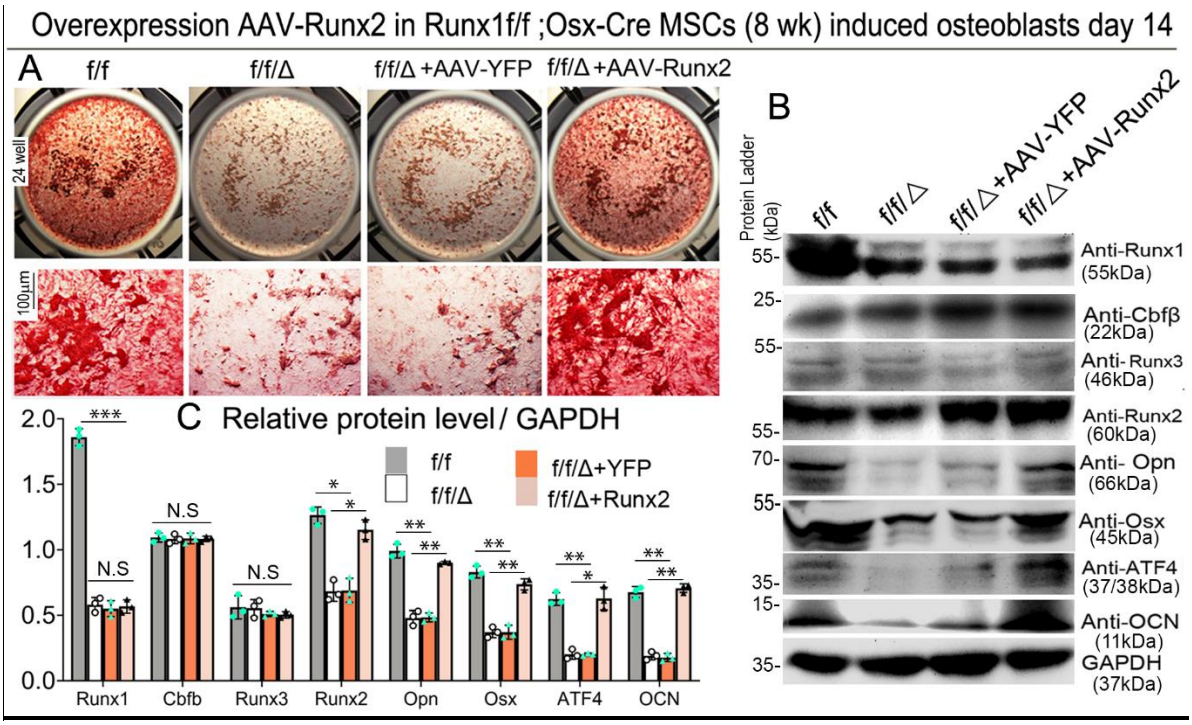

Supplemental Figure 5. Overexpression of Runx2 rescues osteoblast differentiation in Runx1-deficient cells. (A) Runx1 f/f MSCs, Runx1f/f Osx-Cre MSCs, and Runx1f/f Osx-Cre MSCs overexpressing Runx2 mediated by AAV were cultured in osteogenic medium for 14 d, followed by ALP staining to detect osteoblast formation. (B) Protein levels of Runx1, Runx2, Runx3, Cbfβ, Osx, Atf4, Opn and Ocn were analyzed by Western blot analysis on day 14. GAPDH is shown as a control. (C) Quantification of B. n=3 in each group.

Supplementary materials and methods

Supplementary materials and methods

Generation of Runx1$^{f/f}$Osx-Cre mice.

All animal experimentation was carried out according to the legal requirements of the Association for Assessment and Accreditation of the Laboratory Animal Care International and the University of Alabama at Birmingham Institutional Animal Care and Use Committee. Jackson Laboratory, strain name B6.129P2-Runx1tm1Tani/J, JAX no. 008772 were crossed with skeletal tissue cell (including osteoblast precursors, osteoblasts, chondrocytes, and odontoblasts)-specific *Osx-cre* mice (1) (*Tg(Sp7-tTA,tetO-EGFP/cre)1Amc* - Mouse Genome Informatics) Their progeny were crossed with *Runx1$^{f/f}$* mice to obtain *Runx1$^{f/f}$Osx-Cre* mice. In our study, we only use one copy of *Osx-Cre* (*Runx1$^{f/f}$ Osx-Cre/+*) in the CKO mutation. Given one functional allele, heterozygous *Osx -Cre* had no detectable bone phenotype, and served as control groups along with *Runx1$^{f/f}$* mice. Mice were bred in-house and euthanatized by CO_2 asphyxiation. All mice were maintained under a 12 h light–dark cycle with ad libitum access to regular food and water at the UAB Animal Facility. Both male and female mice of each strain were randomly selected into group of five animals each. The investigators were not blinded during allocation, animal handling, and endpoint measurements. Genotyping by PCR was carried out as described (2).

Radiographic Procedures.

For X-ray analysis, radiography was performed using the Faxitron Model MX-20 at 26 kV by the University of Alabama at Birmingham (UAB) Small Animal Bone Phenotyping Core associated with the Center for Metabolic Bone Disease. The microcomputed tomography analysis was

performed to determine the bone mass of fixed femurs by the UAB Small Animal Bone Phenotyping Core associated with the Center for Metabolic Bone Disease.

uCT Analysis

Excised mouse humerus and femurs were scanned using the Scanco CT40 desktop cone-beam micro–CT (mCT) scanner (Scanco Medical AG, Bruttisellen, Switzerland). The trabecular bone scanning was performed from the growth plate (310 slices at 12mm per slice) analyzed using the CT Evaluation Program (v5.0A; Scanco Medical). The scanning and analysis of the cortical bone were performed at the midshaft of the femur and consisted of 25 slices (12 mm per slice).

Skeletal Analysis.

For skeletal preparations, mice were skinned, eviscerated, fixed in 95% (vol/vol) ethanol, cleared in acetone, stained with Alizarin red and/or Alcian blue stains, and sequentially cleared in 1% KOH. Cartilage and mineralized bone were characterized by different colors (blue and red, respectively) after the stain, according to standard protocols (3).

Tissue Preparation

Femurs and tibiae of mice were harvested, skinned, and fixed in 4% (wt/vol) paraformaldehyde overnight. Samples were then dehydrated in ethanol solution and decalcified in 10% (wt/vol) EDTA for 1–4 wk. For paraffin sections, samples were dehydrated in ethanol, cleared in xylene, embedded in paraffin, and sectioned at 6 μm with Leica microtome and mounted on Superfrost Plus slides (Fisher). For frozen sections, samples were infiltrated in 30% (wt/vol) sucrose, embedded in optimal cutting temperature compound, sectioned at 8 μm with a freezing microtome,

and affixed to Superfrost Plus Gold slides (Fisher). Histological analysis was performed including staining with Alcian blue, safranin O, ALP and hematoxylin/eosin (H&E) stains using paraffin sections.

TRAP Staining.

Paraffin sections were stained using the Acid Phosphatase, Leukocyte [tartrate-resistant acid phosphatase (TRAP)] Kit (387A-1KT, Sigma) following the manufacturer's instructions, counterstained with hematoxylin, dehydrated, and mounted. Data are included as graphs of osteoclasts per millimeter of bone perimeter.

Von Kossa Staining.

Von Kossa staining was performed as follows. Cells were washed with Ca2+/Mg2+–free PBS and then fixed on slides in 10% (vol/vol) cold Neutral Formalin solution. We then added 2.5% (wt/vol) silver nitrate solution, and the slides were incubated under UV light for 5–10 min. After incubation, the unincorporated silver nitrate was removed by washing with 5% (wt/vol) sodium thiosulfate. Slides were then mounted. Stain surface per bone surface (BS) area and 5 sections measured using ImageJ software.

ALP staining.

ALP staining was performed as previously described method(4). Slides were deparaffinized and hydrated through a xylene and graded ethanol series, stained with , and counterstained with fast green solution. Slides were then mounted. Stain surface per bone surface (BS) area and 5 sections measured using ImageJ software.

Safranin O staining

Safranin O staining was performed as follows. Slides were deparaffinized and hydrated through a xylene and graded ethanol series, stained with Weigert's iron hematoxylin, rinsed in tap water, and counterstained with fast green solution. Slides were then stained in 0.1% Safranin O solution, dehydrated and mounted.

Proliferation Assay.

To detect proliferating cells in culture, immunochemistry staining was performed according to the manufacturer's instructions. Horseradish peroxidase-conjugated proliferating cell nuclear antigen (PCNA) antibodies (cat. no. 93–1143; Zymed Laboratories Inc.) and Vector DAB (3,3′-diaminobenzidine) kits (cat. no. SK-4100; Vector Laboratories) were used.

Immunohistochemistry.

For immunohistochemistry, samples were embedded in paraffin and sectioned as described previously. The Vector DAB substrate kit (cat. no. SK-4100; Vector Laboratories) was used along with secondary staining kits for mouse (on mouse) and rabbit (cat. no. BMK-2202 and PK6101, respectively; Vector Laboratories) and primary antibodies for Runx1 (sc-365644; Santa Cruz), col2(sc-52658; Santa Cruz), colx (ab58632; Abcam), Runx2 (ab23981; Abcam). For the

quantification of immunohistochemistry, we used NIH ImageJ to perform counts, and the percent of positive cells represents the number of positive cells expressed the targeted gene.

Immunofluorescence.

Samples were embedded in tissue freezing medium, and sections were cut at a thickness of 8 μm with a cryotome. Pictures were taken by Leica confocal microscopes (SP1) and a Zeiss fluorescent microscope (Zeiss Axio Imager). The following antibodies were used: Osterix (ab22552; Abcam), Ocn (ab10911, Abcam), Ihh (MABF23; citeab), PTC1(sc-6149; Santa Cruz), cyclinD1(sc-753; Santa Cruz), PPR(sc-12722; Santa Cruz), Sox9(sc-20095; Santa Cruz). For the quantification of immunofluorescence, we used NIH ImageJ to perform counts, and the percent of positive cells represents the number of positive cells expressed the targeted gene.

Serum P1NP assay.

14-week old mouse serum was collected after 6-hour fasting, and the serum P1NP activity was detected and quantified using the Human Pro-Collagen I alpha Duo Set ELISA (DY6220-05) according to the manufacturer's instructions.

In-vivo calcein labelling.

Calcein labelling was previously described (5). Briefly, 3-month-old mice were intraperitoneally injected with 20mg/kg of calcein in a 2% sodium bicarbonate solution, 8 days and 2 days before killing of mice. Calvarias were fixed in 4% PFA, soaked in 30% glucose in PB, embedded in OCT and frozen sectioned. Mineral apposition rate is the distance between the midpoints of the two labels divided by the time between the midpoints of the interval.

Quantitative Real-Time PCR Analysis.

mRNA was extracted from cultured cells on day14 using TRIzol (Invitrogen) and then reverse-transcribed into cDNA according to the manufacturer's manual (qScript cDNA Synthesis Kit, Quanta Biosciences Inc.). Expressions of osteoblastic marker genes were analyzed by quantitative real-time PCR (qRT-PCR) using the StepOne Real-Time PCR System (Life Technologies). Expression of Atf4, Col1α1, Spp1, Runx2, Sox9, OPG, RANKL, and OCN was analyzed. The primer sequences are available upon request.

Western Blot Analyses.

Protein samples extracted from calvaria derived osteoblasts were prepared in protein lysis buffer, resolved on SDS/PAGE, and electrotransferred onto nitrocellulose membranes. Immunoblotting was performed according to the manufacturer's instructions. Osteoblast- regulators and marker genes including Cbfβ, Runx2, Osterix, Atf4, and Ocn were detected using primary antibodies as follows: rabbit anti-Cbfβ (1:1,000; ab72696, Abcam), rabbit anti-Runx2 (1:2,000; ab23981, Abcam), rabbit anti-Sp7/Osterix (1:1,000; ab22552, Abcam), mouse anti-ATF4 (1:1,000; ab50546, Abcam),rabbit anti-Ocn (1:1,000; ab10911, Abcam); sc-20095, Santa Cruz Biotechnology).Horseradish peroxidase-linked anti-rabbit IgG and horseradish peroxidase-linked anti-mouse IgG were purchased from Cell Signaling (nos. 7074 and 7076).

Data availability

The RNA-Seq data are available upon request. Contact: Yi-Ping Li, Department of Pathology, University of Alabama at Birmingham, E-mail: yipingli@uabmc.edu. All other data are contained within the manuscript.

Supplemental Tables

Table S1. Primers used for qPCR

Gene	Forward primer	Reverse primer
RUNX1	GATGGCACTCTGGTCACCG	GCCGCTCGGAAAAGGACAA
RUNX2	AGAGACCACAATAACCAGCACG	GGCGGCCATATGACTACAAAG
OSX	ATGGCGTCCTCTCTGCTTG	TGAAAGGTCAGCGTATGGCTT
ATF4	ATGGCGCTCTTCACGAAATC	ACTGGTCGAAGGGGTCATCAA
COL1A	CTTGGTGGTTTTGTATTCGATGAC	GCGAAGGCAACAGTCGCT
ALP	AGTTACTGGCGACAGCAAGC	GAGTGGTGTTGCATCGCG
OCN	GAACAGACAAGTCCCACACAG	GAGCTGCTGTGACATCCATAC
RANKL	CAGCATCGCTCTGTTCCTGTA	CTGCGTTTTCATGGAGTCTCA
OPG	TGTCCAGATGGGTTCTTCTCA	CGTTGTCATGTGTTGCATTTCC
HPRT	GGTGGAGATGATCTCTCAACTTTAA	AGGAAAGCAAAGTCTGCATTGTT

Table S2. Primers used for ChIP assay

Gene	Forward primer	Reverse primer
OCN 1	TTGTGCCTCACAACTACCCG	TACACCAGAAGAGGGCGTCA
OCN 2	AGTGCTTGGTCTTTGCTCCA	GCTCTTACCTGCTGAGCCAT
OCN 3	CTTGGGAGTCAGGATGTGTTGAG	ATTCTGCAGTTGTTCCCCAAGT
OCN 4	CAGAGCTGCCCTGAACTGG	CAGGGAGGGAGTGGTCAGTA
OCN 5	CTGAGCACATGACCCCCAAT	ATTGGGGGTCATGTGCTCAG
RUNX2 1	ATGTTCTCTCTGGGCATCCAATC	TGGCAGTGGTCTTTCTAAGTGT
RUNX2 2	GGGTACGTGGACAATGAATGC	TAGTAGAGGTTGCTGAACGTGG
RUNX2 3	TCCTCTGCATGAATAATGACCCTAA	GAGGCTAGACTCATGTTTTACTGT
RUNX2 4	AGTAACCATGGGATGATGGCA	ACGTGGCGGCTCTTACAATA
RUNX2 5	CTAGCCAAATCCTCATGAGTCACAA	GTAAGGCCTTCCTGGCATT

Table S3. Primers used for subcloning

Gene	Primer
RUNX2 F1	CGGGGTACCAGATCACACTGGCACACTTTA
RUNX2 F2	CGGGGTACCCCCTCTTACCTCCACTGTGC
RUNX2 F3	CGGGGTACCTTACAGTTTCTGTTAACCCCCTC
RUNX2 F4	CGGGGTACCAAGCTTGTGATACAATCCCAAGATGCGA
RUNX2 F5	CGGGGTACCAAGCTTGTCAGAGGGAGAAAGGGAGAGAG
RUNX2 R	CCGCTCGAGGCACTATTACTGGAGAGACAGAA

References

1. Rodda, S. J., and McMahon, A. P. (2006) Distinct roles for Hedgehog and canonical Wnt signaling in specification, differentiation and maintenance of osteoblast progenitors. *Development* **133**, 3231-3244
2. Growney, J. D., Shigematsu, H., Li, Z., Lee, B. H., Adelsperger, J., Rowan, R., Curley, D. P., Kutok, J. L., Akashi, K., Williams, I. R., Speck, N. A., and Gilliland, D. G. (2005) Loss of Runx1 perturbs adult hematopoiesis and is associated with a myeloproliferative phenotype. *Blood* **106**, 494-504
3. McLeod, M. J. (1980) Differential staining of cartilage and bone in whole mouse fetuses by alcian blue and alizarin red S. *Teratology* **22**, 299-301
4. Miao, D., and Scutt, A. (2002) Histochemical localization of alkaline phosphatase activity in decalcified bone and cartilage. *J Histochem Cytochem* **50**, 333-340
5. Wu, M., Chen, W., Lu, Y., Zhu, G., Hao, L., and Li, Y. P. (2017) Galpha13 negatively controls osteoclastogenesis through inhibition of the Akt-GSK3beta-NFATc1 signalling pathway. *Nat Commun* **8**, 13700